Anisotropic beam model for analysis and design of passive controlled wind turbine blades

Branner, Kim; Blasques, José Pedro Albergaria Amaral; Kim, Taeseong; Fedorov, Vladimir; Berring, Peter; Bitsche, Robert; Berggreen, Christian

Publication date:
2012

Document Version
Publisher's PDF, also known as Version of record

Anisotropic beam model for analysis and design of passive controlled wind turbine blades

DTU Wind Energy E-Report

K. Branner, J.P. Blasques, T. Kim, V.A. Fedorov, P. Berring,
R.D. Bitsche & C. Berggreen
DTU Wind Energy report E-0001 (EN)
February 2012

DTU Wind Energy
Department of Wind Energy

Author: K. Branner, J.P. Blasques, T. Kim, V.A. Fedorov, P. Berring, R.D. Bitsche & C. Berggreen
Title: Anisotropic beam model for analysis and design of passive controlled wind turbine blades
Department: DTU Wind Energy

DTU Wind Energy report E-0001 (EN)
February 2012

Abstract (max. 2000 char.):

The main objective of the project was, through theoretical and experimental research, to develop and validate a fully coupled, general beam element that can be used for advanced and rapid analysis of wind turbine blades. This is fully achieved in the project and the beam element has even been implemented in the aeroelastic code HAWC2. It has also been demonstrated through a parametric study in the project that a promising possibility with the tool is to reduce fatigue loads through structural couplings. More work is needed before these possibilities are fully explored and blades with structural couplings can be put into production.
A cross section analysis tool BECAS (BEam Cross section Analysis Software) has been developed and validated in the project. BECAS is able to predict all geometrical and material induced couplings. This tool has obtained great interest from both industry and academia.
The developed fully coupled beam element and cross section analysis tool has been validated against both numerical calculations and experimental measurements. Numerical validation has been performed against beam type calculations including Variational Asymptotical Beam Section Analysis (VABS) and detailed shell and solid finite element analyses. Experimental validation included specially designed beams with built-in couplings, a full-scale blade section originally without couplings, which subsequently was modified with extra composite layers in order to obtain measurable couplings. Both static testing and dynamic modal analysis tests have been performed.
The results from the project now make it possible to use structural couplings in an intelligent manner for the design of future wind turbine blades. The developed beam element is especially developed for wind turbine blades and can be used for modeling blades with initial curvature (pre-bending), initial twist and taper. Finally, it have been studied what size of structural couplings can be obtained in current and future blade designs.

EAN 9788792896018
ISBN 978-87-92896-01-8

EFP contract no.:
33033-0075

Project no.:
PSP: 1120167-01

Sponsorship:
The Danish Energy Agency under the Ministry of Climate and Energy

Pages: 41
Figures: 24
Tables: 9
References: 47

Technical University of Denmark
Frederiksborgvej 399
4000 Roskilde
Denmark
Telephone +45 46775024
bcar@dtu.dk
www.vindenergi.dtu.dk

Contents

Sammenfatning (Danish)

Projektets hovedformål var, gennem en teoretisk og eksperimentel forskningsindsats, at forsøge at udvikle et fuldt koblet, generelt og valideret bjælkeelement, der kan bruges til avancerede og hurtige analyser af vindmøllevinger. Dette er til fulde nået og elementet er endda blevet implementeret i HAWC2. Det er også blevet påvist gennem et parameterstudie i projektet, at der er gode muligheder for at reducere udmattelseslasterne ved hjælp af strukturelle koblinger. Mere udviklingsarbejde er dog nødvendigt før disse muligheder er fuldt udforsket og vinger med strukturelle koblinger kan sættes i produktion.

Et tværsnit analyseværktøj (BECAS) er også blevet udviklet og valideret i projektet. BECAS er i stand til korrekt at forudsige alle geometriske og materiale induceret koblinger og værktøjet har skabt stor interesse fra såvel industrien som den akademiske verden.

Både det udviklede fuldt koblede bjælkeelement og tværsnit analyseværktøjet er blevet valideret mod både numeriske beregninger og eksperimentelle målinger. Numerisk validering er udført mod bjælkeberegninger og detaljerede skal- og solid elementmodeller. Eksperimentel validering omfatter specialdesignede bjælker med indbyggede koblinger, en fuld-skala vingesektion oprindeligt uden koblinger, som senere blev modificeret med ekstra kompositlag for at opnå målbare koblinger. Både statisk afprøvning og dynamisk modalanalyse er blevet udført.

Resultaterne fra projektet gør det nu muligt at bruge strukturelle koblinger på en intelligent måde i design af fremtidens vindmøllevinger. Bjælkeelementet er udviklet specielt til vindmøllevinger, og kan bruges til at modellere vinger med initial krumning, twist og taper. Oprindeligt var det en projektidé også at omfatte ikke-lineær deformation af tværsnittet, men dette har vist sig at være for ambitiøst i forhold til projektets omfang og vil derfor kræve mere forskning, før det er muligt. Til gengæld er elementet blevet implementeret og afprøvet i HAWC2, hvilket ikke var med i den oprindelige projektplan.

1 Introduction

This report is a summary of the results obtained in the project: Anisotropic beam model for analysis and design of passive controlled wind turbine blades (ANBAVI). The project was supported by the Danish Energy Authority through the 2007 Energy Research Programme (EFP 2007) and has journal no. 33033-0075. The project has been running from spring 2007 to the end of 2011.

Being a summary report, this report only contains a brief collection of the research topics and the major results. For more details, see the publications listed at the end of this report.

1.1 Motivation and problem description

The project is motivated by the vision of being able to provide passive control of the dynamic behavior of wind turbine blades by utilizing the anisotropic properties of composite materials in an intelligent manner. To obtain this vision, one of the main building blocks needed, in the numerical tool package, is a general, fully coupled and validated beam element. Also needed are effective and exact methods for determination of stiffness and mass coefficients for the fully coupled beam element based on 3D geometry and material data for the blade. The main purpose of the project described in this report is to develop such a beam element with exact prediction of stiffness and mass coefficients.

In order to include the effect from anisotropic materials in aeroelastic calculations a beam based model which includes all couplings is needed. The model must be solved fast and efficiently as often thousands of time series must be analyzed in order to generate the load basis for an onshore or offshore wind turbine.

An expected spin-off from the project is increased confidence in estimating the risk of flutter and other dynamic instabilities. Instability phenomena come from the dynamic behavior of the blade in interaction with the dynamic forces. It is therefore possible to avoid these dynamic instabilities by changing the dynamic properties of the blade by structural design. The risk of flutter is very much governed by the ratio between flapwise bending and torsion stiffness and to some extend by the bend-twist coupling. It is therefore important to be able to calculate these stiffness coefficients correctly. Experience has shown that especially calculation of the torsional stiffness is encumbered with some uncertainty. The project has contributed to decrease this uncertainty by validating the developed models against experimental results.

Furthermore, a fully coupled beam element can be used in aeroelastic calculations to design the structure in order to reduce fatigue loading of the blade. Modern pitch-regulating wind turbines use control systems to reduce the blade loads. However, these systems are too slow to react to sudden wind changes. There is therefore large interest in building active or passive control systems into the blades to reduce especially fatigue loads. Passive systems are much more robust against operation interruptions and it is therefore obvious to use the anisotropic material properties for composites to optimize the load reduction behavior of the blades.

1.2 Basic beam theory

A prismatic Timoshenko 3D beam element is presently used in the aerolastic code HAWC2. The beam element can be defined by the following constitutive relation:

$$\begin{pmatrix} F_x \\ F_y \\ F_z \\ M_x \\ M_y \\ M_z \end{pmatrix} = \begin{pmatrix} GA{\cdot}k_x & 0 & 0 & 0 & 0 & 0 \\ 0 & GA{\cdot}k_y & 0 & 0 & 0 & 0 \\ 0 & 0 & AE & 0 & 0 & 0 \\ 0 & 0 & 0 & EI_x & 0 & 0 \\ 0 & 0 & 0 & 0 & EI_y & 0 \\ 0 & 0 & 0 & 0 & 0 & GJ \end{pmatrix} \cdot \begin{pmatrix} \gamma_x \\ \gamma_y \\ \varepsilon_z \\ \kappa_x \\ \kappa_y \\ \kappa_z \end{pmatrix}$$

As illustrated, the constitutive matrix has only diagonal terms. GAk_x and GAk_y are the shear stiffness in the x- and y-directions respectively. AE is the axial stiffness, EI_x and EI_y are the bending stiffness about the x- and y-axis respectively. Finally, GJ is the torsional stiffness of the beam element.

The beam element is described according to the elastic axis and orientated as the principle axes which decouples bend-bend couplings (EI_{xy}). This element can be modified to account for the location of the shear center which results in a few off-diagonal terms in the constitutive matrix.

In order to improve the results from HAWC2 a new 3D anisotropic beam element is implemented into the code. This element can be fully populated which means that it accounts for all couplings. These couplings can come from the material lay-up and the geometry of the blade section. The constitutive relation of the new element is illustrated below:

$$\begin{pmatrix} F_x \\ F_y \\ F_z \\ M_x \\ M_y \\ M_z \end{pmatrix} = \begin{pmatrix} k_{11} & k_{12} & k_{13} & k_{14} & k_{15} & k_{16} \\ k_{21} & k_{22} & k_{23} & k_{24} & k_{25} & k_{26} \\ k_{31} & k_{32} & k_{33} & k_{34} & k_{35} & k_{36} \\ k_{41} & k_{42} & k_{43} & k_{45} & k_{45} & k_{46} \\ k_{51} & k_{52} & k_{53} & k_{54} & k_{55} & k_{56} \\ k_{61} & k_{62} & k_{63} & k_{64} & k_{65} & k_{66} \end{pmatrix} \cdot \begin{pmatrix} \gamma_x \\ \gamma_y \\ \varepsilon_z \\ \kappa_x \\ \kappa_y \\ \kappa_z \end{pmatrix}$$

2 Development of cross section analysis tool

2.1 Introduction

Cross section analysis tools are commonly employed in the development of beam models for the analysis of long slender structures. These types of models can be very versatile when compared against their equivalent counterparts as they generally offer a very good compromise between accuracy and computational efficiency. When suited, beam models

can be advantageously used in an optimal design context (see, e.g., Ganguli and Chopra, 1995, Li et al., 2008, Blasques and Stolpe, 2010) or in the development of complex multiphysics codes. Wind turbines aeroelastic codes, for example, commonly rely on these types of models for the representation of most parts of the wind turbine, from the tower to the blades (see, e.g., Hansen et al., 2006, Chaviaropoulos et al., 2006). In particular, the development of beam models which correctly describe the behaviour of the wind turbine blades have been the focus of many investigations. The estimation of the properties of these types of structures becomes more complex as the use of different combinations of advanced materials becomes a standard. See Figure 1 for a schematic description of the use of beam elements to analyze the response of wind turbine blades. It is therefore paramount to develop cross section analysis tools which can correctly account for all geometrical and material effects.

BECAS (BEam Cross section Analysis Software) is a general purpose cross section analysis tool specifically developed within this project for these types of applications. BECAS is able to handle a large range of arbitrary section geometries and correctly predict the effects of inhomogeneous material distribution and anisotropy. Based on a definition of the cross section geometry and material distribution, BECAS is able to determine the cross section stiffness properties while accounting for all the geometrical and material induced couplings. These properties can consequently be utilized in the development of beam models to accurately predict the response of wind turbine blades with complex geometries and made of advanced materials.

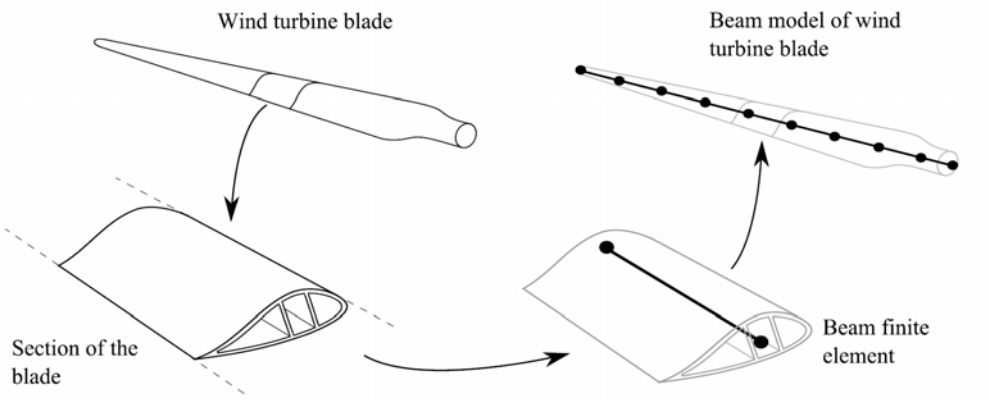

Figure 1 Schematic description illustrating the use of beam finite element models to analyse the response of wind turbine blades.

BECAS is based on the theory originally presented by Giavotto et al., 1983 for the analysis of inhomogeneous anisotropic beams. The theory leads to the definition of two types of solutions of which, and in accordance to De Saint-Venant's principle, the non-decaying solutions are the basis for the evaluation of the cross section stiffness properties. A slight modification to the theory was introduced later by Borri and Merlini, 1986 where the concept of intrinsic warping is introduced in the derivation of the cross section stiffness matrix. Despite the modifications, no difference in the results was reported. The theory was subsequently extended by Borri et al., 1992 to account for large displacements, curvature and twist. Ghiringhelli and Mantegazza, 1994 presented an implementation of the theory for commercial finite element codes. Finally Ghiringhelli,

1997a, Ghiringhelli, 1997b and Ghiringhelli et al., 1997 presented a formulation incorporating thermoelastic and piezo-electric effects, respectively. The validation results presented throughout each of the previously mentioned publications highlight the robustness of the method in the analysis of the stiffness and strength properties of anisotropic and inhomogeneous beam cross sections. According to Yu et al., 2002a implementations of this theory have been in fact used as a benchmark for the validation of any new tool emerging since the early 1980's (see, e.g., Yu et al., 2002a, Yu et al., 2002b and Chen et al., 2010).

Many other cross section analysis tools have been described in the literature. The reader is referred to Jung et al., 1999 and Volovoi et al., 2001 for an assessment of different cross section analysis tools. Nonetheless, at this stage the Variational Asymptotic Beam Section analysis commercial package VABS by Yu et al., 2002a is perhaps the state of the art for these type of tools. VABS has been extensively validated (see Yu et al., 2002a, Yu et al., 2002b and Chen et al., 2010) and has therefore been used as the benchmark for the validation of BECAS. It was shown then that the cross section properties estimated by both tools are in very good agreement.

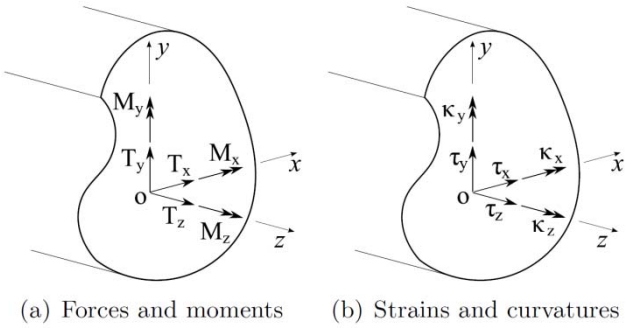

Figure 2 Cross section coordinate system, forces and moments (a) and corresponding strains and curvatures (b).

2.2 Theory

This section presents a brief description of the theory underlying BECAS and described in Blasques and Lazarov, 2011.

2.2.1 Assumptions

For a linear elastic beam there exists a linear relation between the cross section generalized forces $\mathbf{T}$ and moments $\mathbf{M}$ in $\boldsymbol{\theta} = [\ \mathbf{T}^T\ \mathbf{M}^T\ ]^T$ (cf. Figure 2 (a)), and the resulting strains $\boldsymbol{\tau}$ and curvatures $\boldsymbol{\kappa}$ in $\boldsymbol{\psi} = [\ \boldsymbol{\tau}^T\ \boldsymbol{\psi}^T\ ]^T$ (Figure 2 (b)). This relation is given in its stiffness form as $\boldsymbol{\theta} = \mathbf{K}\boldsymbol{\psi}$, or

$$\begin{bmatrix} T_x \\ T_y \\ T_z \\ M_x \\ M_y \\ M_z \end{bmatrix} = \begin{bmatrix} K_{11} & K_{12} & K_{13} & K_{14} & K_{15} & K_{16} \\ K_{21} & K_{22} & K_{23} & K_{24} & K_{25} & K_{26} \\ K_{31} & K_{32} & K_{33} & K_{34} & K_{35} & K_{36} \\ K_{41} & K_{42} & K_{43} & K_{44} & K_{45} & K_{46} \\ K_{51} & K_{52} & K_{53} & K_{54} & K_{55} & K_{56} \\ K_{61} & K_{62} & K_{63} & K_{64} & K_{65} & K_{66} \end{bmatrix} \begin{bmatrix} \tau_x \\ \tau_y \\ \tau_z \\ \kappa_x \\ \kappa_y \\ \kappa_z \end{bmatrix}$$

where **K** is the 6 x 6 cross section stiffness matrix. In the most general case, considering material anisotropy and inhomogeneity, all the 21 stiffness parameters in **K** may be required to describe the deformation of the beam cross section.

The transverse force components $\mathbf{T} = [\ T_x\ T_y\ T_z\ ]^T$ represent the shear in the x direction, the shear in the y, and the tension force in the z direction, respectively. The components of the $\mathbf{M} = [\ M_x\ M_y\ M_z\ ]^T$ represent the bending moment in around the x axis, the bending component around the y axis, and the torsional moment around the z axis. The shear component $\boldsymbol{\tau} = [\ \tau_x\ \tau_y\ \tau_z\ ]^T$ is composed of the shear strains τ_x and τ_y, and the tension strain τ_z. The components of the vector of curvatures $\boldsymbol{\kappa} = [\ \kappa_x\ \kappa_y\ \kappa_z\ ]^T$ are the bending curvatures κ_x and κ_y, and the twist rate κ_z.

2.2.2 Cross section equilibrium equations

The theory underlying BECAS assumes that the cross section deformation is defined by a superimposition of the rigid body motions **r** (translations and rotations) and warping deformations **g**. The first step in the derivation consists of establishing the cross section equilibrium equations. The equations are derived in a finite element context. The cross section face is discretized using two dimensional finite elements. The three-dimensional warping deformations in **g** are approximated by the nodal deformations of the finite element mesh **u**. By application of the principle of virtual work, it is possible to establish the finite element form of the cross section equilibrium equations, defined as

$$\begin{cases} \mathbf{E}\frac{\partial \mathbf{u}}{\partial z} + \mathbf{R}\frac{\partial \boldsymbol{\psi}}{\partial z} = 0 \\ \mathbf{R}^T\frac{\partial \mathbf{u}}{\partial z} + \mathbf{A}\frac{\partial \boldsymbol{\psi}}{\partial z} = \frac{\partial \boldsymbol{\theta}}{\partial z} \end{cases}$$

$$\begin{cases} \mathbf{E}\mathbf{u} + \mathbf{R}\boldsymbol{\psi} = \left(\mathbf{C} - \mathbf{C}^T\right)\frac{\partial \mathbf{u}}{\partial z} + \mathbf{L}\frac{\partial \boldsymbol{\psi}}{\partial z} \\ \mathbf{R}^T\mathbf{u} + \mathbf{A}\boldsymbol{\psi} = -\mathbf{L}^T\frac{\partial \mathbf{u}}{\partial z} + \boldsymbol{\theta} \end{cases}$$

$$\frac{\partial \boldsymbol{\theta}}{\partial z} = \mathbf{T}_r^T\boldsymbol{\theta}$$

The matrices **E**, **A**, **R**, **L**, **C**, and $\mathbf{T}_r$ are defined in Blasques and Lazarov, 2011. For a given vector $\boldsymbol{\theta}$ it is possible using the equations above (after application of the correct contraints) to determine the cross section warping displacements **u** and the cross section generalized strains $\boldsymbol{\psi}$.

2.2.3 Cross section stiffness matrix

Consider the case where the cross section equilibrium equations are solved for different right-hand sides each corresponding to setting one of the entries of $\boldsymbol{\theta}$ to unity and the remaining to zero. This procedure is similar to the stiffness method in the finite element method. It can be realized by replacing the cross section load vector $\boldsymbol{\theta}$ by the 6x6 identity matrix $\mathbf{I}_6$ and solving the following set of equations

$$\begin{cases} \mathbf{EX} + \mathbf{RY} = \left(\mathbf{C} - \mathbf{C}^T\right) \frac{\partial \mathbf{X}}{\partial z} + \mathbf{L} \frac{\partial \mathbf{Y}}{\partial z} \\ \mathbf{R}^T \mathbf{X} + \mathbf{AY} = -\mathbf{L}^T \frac{\partial \mathbf{X}}{\partial z} + \mathbf{I}_6 \end{cases}$$

$$\begin{cases} \mathbf{E} \frac{\partial \mathbf{X}}{\partial z} + \mathbf{R} \frac{\partial \mathbf{Y}}{\partial z} = 0 \\ \mathbf{R}^T \frac{\partial \mathbf{X}}{\partial z} + \mathbf{A} \frac{\partial \mathbf{Y}}{\partial z} = \mathbf{T}_r^T \end{cases}$$

where the resulting solution matrices **U**, d**U**/dz, **Ψ** and d**Ψ**/dz have six columns each corresponding to each of the six right-hand sides. Using the solutions from the system of linear equations above and based on the complimentary form of the internal virtual energy of the cross section it is possible to determine the cross section compliance matrix **F** defined as

$$\mathbf{F} = \begin{bmatrix} \mathbf{X} \\ \frac{\partial \mathbf{X}}{\partial z} \\ \mathbf{Y} \end{bmatrix}^T \begin{bmatrix} \mathbf{E} & \mathbf{C} & \mathbf{R} \\ \mathbf{C}^T & \mathbf{M} & \mathbf{L} \\ \mathbf{R}^T & \mathbf{L}^T & \mathbf{A} \end{bmatrix} \begin{bmatrix} \mathbf{X} \\ \frac{\partial \mathbf{X}}{\partial z} \\ \mathbf{Y} \end{bmatrix}$$

where **M** is defined in Blasques and Lazarov, 2011. The corresponding stiffness matrix **K** can be computed as

$$\mathbf{K} = \mathbf{F}^{-1}$$

This result can be used to generate beam finite element models for which the strains can be exactly described by the six strain parameters in **ψ**. The material may be anisotropic, inhomogeneously distributed, and the reference coordinate system may be arbitrarily located. The stiffness matrix **K** will correctly account for any geometrical or material couplings.

2.2.4 Shear center and elastic center positions, and elastic axes

Having determined the cross section stiffness matrix it is possible to determine the locations of the shear and elastic centers. The shear center $\mathbf{s}_c = (x_s, y_s)$ is defined as the point at which a load applied parallel to the plane of the section will produce no torsion (i.e., $\kappa_z = 0$). The shear center is defined as

$$x_s = -\frac{F_{62} + F_{64}(L - z)}{F_{66}}$$
$$y_s = \frac{F_{61} + F_{65}(L - z)}{F_{66}}$$

where F_{ij} is the entry ij of the compliance matrix **F**. From the previous equation it can be seen that the shear center is not a property of the cross section. Instead, in the case where the entries F_{64} and F_{65} associated with the bend-twist coupling are not zero, the position of the shear center varies linearly along the beam length.

The elastic center $\mathbf{e}_c = (x_e, y_e)$ is defined as the point where a force applied normal to the cross section will produce no bending curvatures (i.e., (i.e., $\kappa_x = \kappa_y = 0$). The position of the elastic center is defined as

$$x_e = -\frac{-F_{44}F_{53} + F_{45}F_{43}}{F_{44}F_{55} - F_{45}^2}$$
$$y_e = -\frac{F_{43}F_{55} - F_{45}F_{53}}{F_{44}F_{55} - F_{45}^2}$$

Often, the bending stiffnesses are measured along the elastic axis such that the coupling between the bending in x and y directions is uncoupled, i.e., $K_{45} = K_{54} = 0$. In BECAS, the orientation of the elastic axis is determined by solving the following eigenvalue problem

$$\left(\begin{bmatrix} K_{44} & K_{45} \\ K_{54} & K_{55} \end{bmatrix} - \lambda \mathbf{I} \right) \mathbf{v} = 0$$

The solution to the eigenvalue problem above yields the eigenvectors $\mathbf{v}_1$ and $\mathbf{v}_2$ which indicate the orientation of the elastic axes. The angle α_{ea} between the reference coordinate system and the elastic axes is determined as

$$\alpha_{ea} = \arctan\left(\frac{v_{1,2}}{v_{1,1}}\right);$$

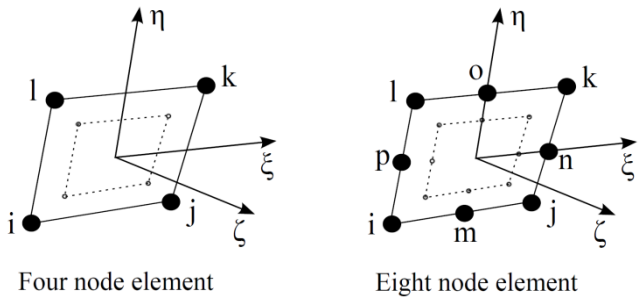

Four node element Eight node element

Figure 3 Node numbering convention and position of Gauss points for the four and eight node finite elements which may be used in the cross section finite element mesh.

2.2.5 Cross section finite element mesh

In BECAS both four and eight node elements can be used in the cross section finite element mesh. The four node element uses linear interpolation while the eight node elements uses quadratic interpolation. Note that although these are similar to the typical two-dimensional elements, in this case there are three degrees of freedoms per node corresponding to the displacements in the three directions x, y, and z. The node ordering and position of the Gauss points for both elements are presented in Figure 3. The triangular forms of these elements can be obtained by simply defining coinciding nodes.

3 Validation of the cross section analysis tool

In this section numerical results obtained using BECAS are discussed. The resulting entries of the cross section stiffness matrix **K** as well as the positions of the shear and elastic center are compared to the results from VABS - the Variational Asymptotic Beam Section analysis code (Yu et al., 2002a, Yu et al., 2002b). VABS has been extensively validated against different cross section analysis tools and analytical results (see Yu et

al., 2002a, Yu et al., 2002b, Chen et al., 2010 and Volovoi et al., 2001) and it is therefore a benchmark for validation of new cross section analysis codes.

The numerical experiments presented for validation have been chosen so that different material and geometrical effects are analyzed. From a material properties standpoint, the aim is to analyze the effect of material anisotropy and its inhomogeneous distribution over the cross section. In terms of cross section geometry we look at solid, thin-walled, open and multi-cell cross sections. Hence, four different cross section geometries have been considered - solid square, cylinder, half cylinder and three cells. All the combinations of cross section geometry and material properties are summarized in Table 1.

Table 1 Catalogue of problems used for the validation of BECAS against VABS (see Blasques and Lazarov, 2011).

Ref.	Geometry	Material
S1	Solid square	Isotropic
S2	Solid square	Isotropic #1 + Isotropic #2
S3	Solid square	Orthotropic
C1	Cylinder	Isotropic #1
C2	Half-cylinder	Isotropic #1
C3	Cylinder	Isotropic #1 + Isotropic #2
C4	Cylinder (layered)	Isotropic #1 + Isotropic #2
T1	Three-cells	Isotropic #1
T2	Three-cells	Isotropic #1 + Orthotropic

All results obtained using BECAS were found to be in perfect agreement with VABS for all the cross sections analyzed (see examples of the results in Figure 4 from Blasques and Lazarov, 2011). These results strongly indicate that the BECAS implementation has been correctly performed and is ready for use in an aeroelastic tailoring framework.

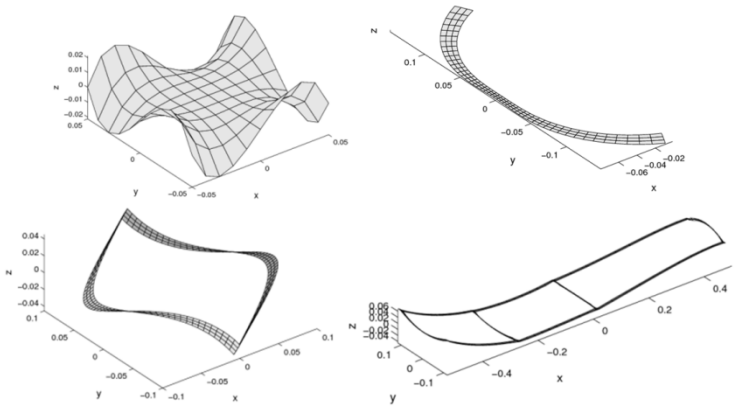

Figure 4 Examples of the cross sections analyzed for the validation of BECAS. All results were found to be in very good agreement with VABS. The plots present the deformed shape of the cross sections for different load cases.

Figure 5 presentes an example of the application of BECAS in the analysis of the cross section properties of a generic wind turbine blade cross section. Using BECAS it is possible to estimate the position of the shear and elastic centers correctly, and the orientation of the elastic axis.

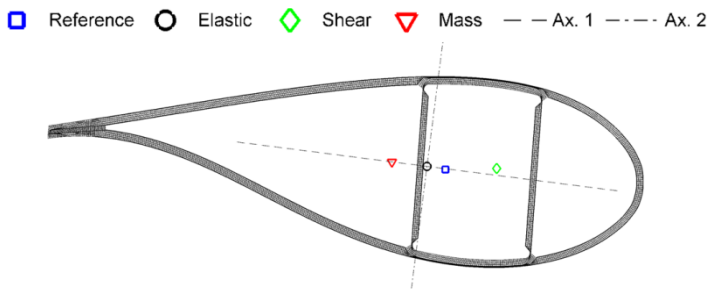

Figure 5 Wind turbine cross section finite element mesh and shear and elastic center postions, and elastic axis orientations as calculated by BECAS.

Finally, BECAS has been used in an optimization framework by Blasques and Stolpe, 2012, and Blasques, 2012. The authors used topology optimization techniques to determine optimal cross section topologies and material distribution in the design of laminated composite beams. The applicability of the method was attested in the optimal design of a wind turbine blade (see Blasques and Stolpe, 2012).

4 Determination of coupling coefficients from numerical models and tests

4.1 Introduction

In the following presented a short summery of one of the methods for determining the constitutive matrix is presented. The method is based on the paper *Identification and Use of Blade Physical Properties* by Malcolm and Laird, 2005 and is further developed in this project. This method works by performing six different load cases on a full FE-model and then determines a single set of displacements and rotations (three displacements and three rotations) of each beam element.

The fully populated Timoshenko stiffness matrix of the beam element can then be obtained from these displacements and rotations.

4.2 The Beam Property Extraction (BPE) method

A complete FE-model of a wind turbine blade typically consists of thousands of composite shell elements and also solid elements for some FE-models.

The FE-models are very complex since they are used for examining stresses/strains, local and global deflections, etc. But the FE-models are too detailed for aeroelastic analysis that these analyses are normally based on a series of equivalent three-dimensional beam elements that represent the full blade. The beam elements must accurately represent the real full blade global behavior such as shear deformation, bend-twist coupling, offsets between the elastic and shear centers, etc.

4.2.1 Extraction of the equivalent beam properties

Since a wind turbine blade has a big cross sectional variation when going from the root to the tip, the equivalent beam elements will also have widely different cross sectional properties.

The full wind turbine blade can be described by dividing the blade into several beam elements (with constant cross sectional properties).

A quarter of the full 12x12 stiffness matrix [K] for the beam elements can be determined by applying a series of six static loads (two shear forces, one axial force and two bending moments and one torsional moment) at the tip of the blade. The quarter determined is the one that defines one end of the element with respect to the other, the right with respect to the left. The blade is divided into a number of elements which stiffness matrixes can be determined by the elements internal forces/moments and their relative displacements rotations.

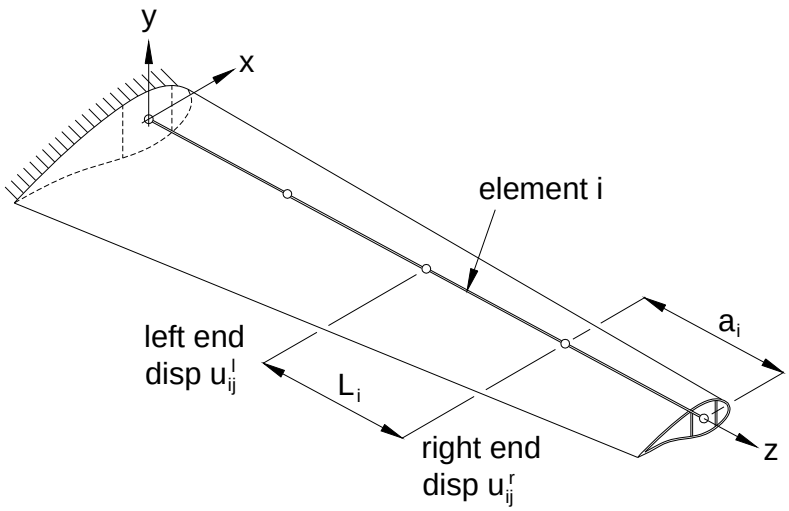

Figure 6 Equivalent beam element for a 3D blade model.

The relative displacements and rotations for the six load cases (j = 1,..6) can be determined by:

$$u_{ijx}^{rl} = u_{ijx}^{r} - u_{ijx}^{l} - \theta_{ijy}^{l} \cdot L_i \qquad u_{ijy}^{rl} = u_{ijy}^{r} - u_{ijy}^{l} - \theta_{ijx}^{l} \cdot L_i \qquad u_{ijz}^{rl} = u_{ijz}^{r} - u_{ijz}^{l}$$

$$\theta_{ijx}^{rl} = \theta_{ijx}^{r} - \theta_{ijx}^{l} \qquad \theta_{ijy}^{rl} = \theta_{ijy}^{r} - \theta_{ijy}^{l} \qquad \theta_{ijz}^{rl} = \theta_{ijz}^{r} - \theta_{ijz}^{l}$$

L_i is the length of element i and a_i is the distance from the applied loads to the element.

Since the locations of the elastic and shear centers are not known one must select a global reference coordinate system and a global reference axis along the blade. The longitudinal pitch axis is an obvious choice for reference but other locations can also be used.

After selecting a reference coordinate system the static loads can be applied with respect to the reference. The relative deflections and rotations are determined with respect to the reference.

The series of static loads consists of two transverse forces (F_x and F_y), an axial force (F_z), two pure bending moments (M_x and M_y) and a torsional moment (M_z).The elements stiffness matrices [K_i] are calculated in the following way:

$$F_i = K_i \cdot U_i \quad \Rightarrow$$

$$\begin{pmatrix} F_x & 0 & 0 & 0 & 0 & 0 \\ 0 & F_y & 0 & 0 & 0 & 0 \\ 0 & 0 & F_z & 0 & 0 & 0 \\ 0 & -F_y \cdot a_i & 0 & M_x & 0 & 0 \\ F_x \cdot a_i & 0 & 0 & 0 & M_y & 0 \\ 0 & 0 & 0 & 0 & 0 & M_z \end{pmatrix} = K_i \cdot \begin{pmatrix} u_{i1x}^{rl} & u_{i2x}^{rl} & u_{i3x}^{rl} & u_{i4x}^{rl} & u_{i5x}^{rl} & u_{i6x}^{rl} \\ u_{i1y}^{rl} & u_{i2y}^{rl} & u_{i3y}^{rl} & u_{i4y}^{rl} & u_{i5y}^{rl} & u_{i6y}^{rl} \\ u_{i1z}^{rl} & u_{i2z}^{rl} & u_{i3z}^{rl} & u_{i4z}^{rl} & u_{i5z}^{rl} & u_{i6z}^{rl} \\ \theta_{i1x}^{rl} & \theta_{i2x}^{rl} & \theta_{i3x}^{rl} & \theta_{i4x}^{rl} & \theta_{i5x}^{rl} & \theta_{i6x}^{rl} \\ \theta_{i1y}^{rl} & \theta_{i2y}^{rl} & \theta_{i3y}^{rl} & \theta_{i4y}^{rl} & \theta_{i5y}^{rl} & \theta_{i6y}^{rl} \\ \theta_{i1z}^{rl} & \theta_{i2z}^{rl} & \theta_{i3z}^{rl} & \theta_{i4z}^{rl} & \theta_{i5z}^{rl} & \theta_{i6z}^{rl} \end{pmatrix}$$

The first column in the displacement matrix U is the displacements from load case F_x j=1, the second is from load case F_y (j=2),.. and the last is from load case M_z (j=6).

$$K_i = F_i \cdot \left(U_i\right)^{-1}$$

By applying Timoshenko beam theory the following equations can be derived:

$$K^{-1} \cdot Q^{-1} = k^{-1} \cdot H \cdot Q^{-1} + E \cdot k^{-1}$$

H, E and Q are defined in Malcolm and Laird, 2005 in terms of the elements along the blade axis. The constitutive matrix [k], which is the input to HAWC2, can be determined by using Lyapunov's method.

4.2.2 Determining the cross sectional displacements and rotations

Each cross section in an FE-model will potentially have hundreds of degrees-of-freedom and all these degrees-of-freedom must be described by the six degrees-of-freedom (the three displacements and rotations) according to the reference coordinate system.

In Malcolm and Laird, 2005 a least squares algorithm is applied where a plan is fitted through the finite element nodal displacements. The description of the complete algorithm/approach is very limited in the paper.

In this work the commercial software MSC.Patran/Nastran is used and the cross sectional displacements and rotations are determined by applying a MPC (Multi Point Constrain) element of the type RBE3. The RBE3 element creates a link between one dependent node (master node) and a number of independent nodes. RBE3 is a linear interpolation element which means that the displacement and rotation of the dependent node is governed by the independent nodes on the cross section. Furthermore, the RBE3 element does not constrain the cross section, meaning that it can deform unaffectedly by the element. The dependent node is created in the center of the spar and then linked to all the surrounding nodes in the cross section as shown in Figure 7.

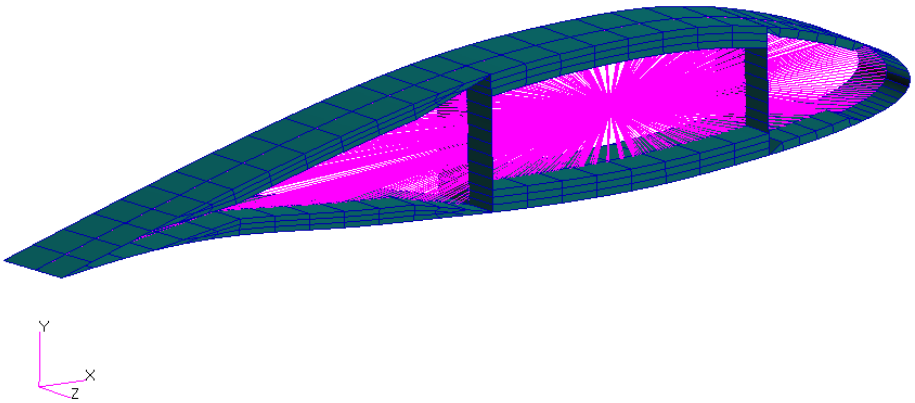

Figure 7 MPC element of the type RBE3 applied to a cross section of the model.

4.2.3 A simple study case

In Malcolm and Laird, 2005 the method is tested on a simple steel tube where analytical equations for the stiffness properties are well known. The method results in very imprecise shear stiffness properties (deviations up to 125%) while bending and torsional stiffness are determined very accurately. Other cross sectional properties such as location of elastic center, shear center and orientations of principal axis are not reported.

After further development of the method the same test cases is investigated. A MSC.Patran/Nastran model of the steel type is generated and MPC elements of the type RBE3 is applied to determine the displacements and rotations which are the input to the BPE-method. The structure was meshed with 20 elements circumferentially and 50 longitudinally. The elements were 8-node quadrilateral shell elements which were located in the material mid-thickness.

To test the robustness of this approach were the master node in the RBE3 elements offset 250mm in the x-direction and -62.5mm in the y-direction and the tube was then rotated 10° about the z-axis. Presented below are the results of steel tube study case.

$$k_{3\_BPE} = \begin{pmatrix} 765.69 & 0 & -0 & 0 & -0 & 0 \\ 0 & 107.89 & 0 & 0 & -0 & -0 \\ -0 & 0 & 2625 & 0 & 0 & -0 \\ 0 & 0 & 0 & 35.55 & 0 & 0 \\ -0 & -0 & 0 & 0 & 306.25 & 0 \\ 0 & -0 & -0 & 0 & 0 & 39.08 \end{pmatrix} \cdot 10^6 \qquad k_{analytical} = \begin{pmatrix} 767.2 & 0 & 0 & 0 & 0 & 0 \\ 0 & 110.7 & 0 & 0 & 0 & 0 \\ 0 & 0 & 2625 & 0 & 0 & 0 \\ 0 & 0 & 0 & 35.55 & 0 & 0 \\ 0 & 0 & 0 & 0 & 306.26 & 0 \\ 0 & 0 & 0 & 0 & 0 & 40.38 \end{pmatrix} \cdot 10^6$$

Where stiffness properties determined by the BPE-method are presented to the left and analytical values are presented to the right.

The constitutive matrix for the beam element is transformed (translation) to the elastic center and transformed (rotated) according to the principle axes. The diagonal in the blue box shows the shear stiffnesses in the x- and y-direction (GAk_x and GAk_y [N]). The diagonal in the green box shows the following cross sectional properties; AE [N], EI_x [Nm^2], EI_y [Nm^2] and GJ [Nm^2].

An excellent agreement between all the analytical and numerical stiffness properties is found. Based on this study it is indicated that the cross sectional displacements and

rotations are determined with a higher accuracy using the present method compared with the least squares algorithm applied by Malcolm and Laird, 2005.

A number of FE-models with more complex beam structures were analyzed in this work and their stiffness properties were determined by applying the BPE-method. The result showed that for beam structures with double symmetric cross sections the method determined the different stiffness properties in excellent agreement with theoretical values.

For the beam structures analyzed with highly asymmetric and anisotropic cross sections the constitutive matrixes determined by BPE-method were not completely symmetric which is an error in the method. The matrix should theoretically be completely symmetric.

However, if the asymmetric "noise" in the constitutive matrixes were neglected the main stiffness properties determined by the method for all beam structures analyzed were in good agreement with theoretical values.

4.2.4 Determination of stiffness properties for a wind turbine blade section

In this work a detailed MSC.Patran/Nastran finite element model of an 8 meter long blade section, provided by Vestas Wind Systems A/S, was applied to test the BPE-method. The model consists of a combination of 20-noded solid elements (Hex20) and 8-noded shell elements (Quad8). The solid elements are applied to model, the core material and adhesive bonds while the sandwich face layers and caps are models with layered shell elements.

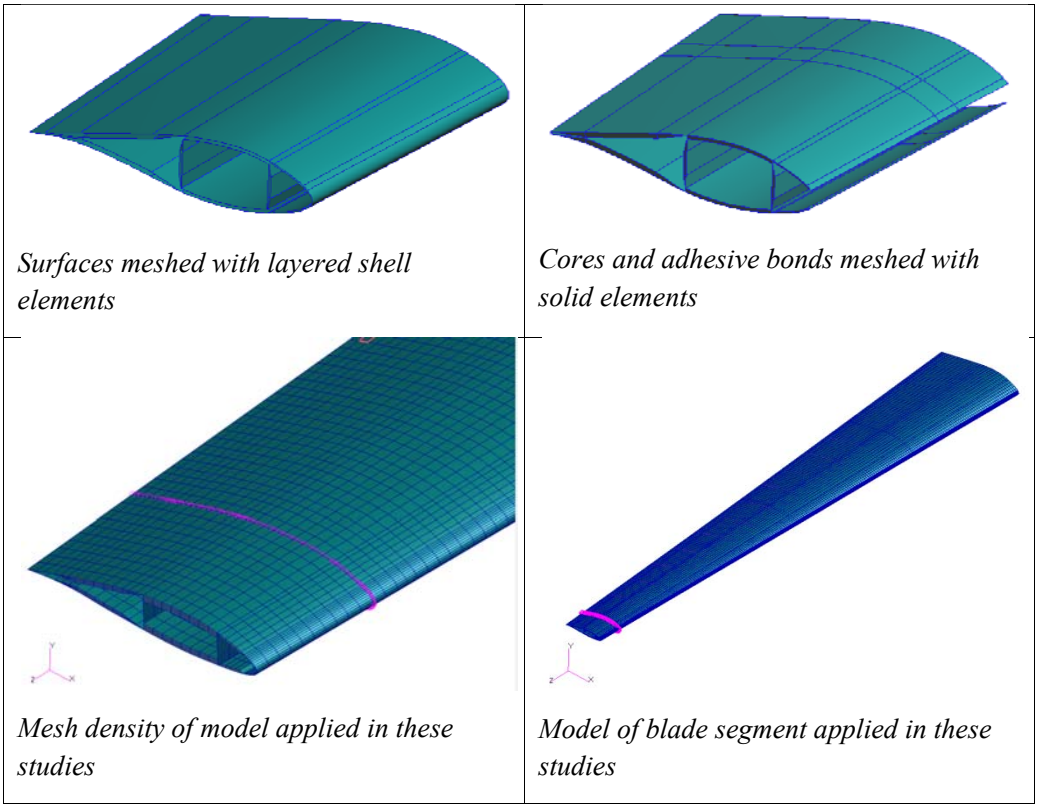

Surfaces meshed with layered shell elements

Cores and adhesive bonds meshed with solid elements

Mesh density of model applied in these studies

Model of blade segment applied in these studies

Figure 8 Model of wind turbine blade segment.

Numerical results of the global response (cross sectional displacements and rotations) were compared with a large experimental test campaign where different load configurations were applied, including flapwise, edgewise and torsional loading. For more details about the model and experimental test campaign see Berring et al., 2007, Branner et al., 2007, Luczak et al., 2011.

4.2.5 Results of the BPE-method applied on the blade section

The blade model was split up into seven beam elements of equal length. Presented in Table 2 are the estimated locations of elastic center (ec), shear center (sc) and orientation of principle axis.

Table 2 Determined location of elastic center, shear center and orientation of principle axis.

BPE-6x6-method	x-direction (Xec), location of elastic center [m]	y-direction (Yec), location of elastic center [m]	x-direction (Xsc), location of shear center [m]	x-direction (Ysc), location of shear center [m]	Orientation of principle axes [degrees]
BPE-element 1	-0,030679	-0,002106	0,012362	0,010672	4,078
BPE-element 2	-0,031869	-0,002083	0,031528	0,013233	3,820
BPE-element 3	-0,033006	-0,002458	0,012372	0,021082	3,476
BPE-element 4	-0,034225	-0,002149	0,024876	0,021177	3,117
BPE-element 5	-0,038277	-0,001612	0,049214	0,019389	2,665
BPE-element 6	-0,042044	-0,001007	0,079807	-0,016598	2,126
BPE-element 7	-0,046685	-0,000450	0,070049	-0,042334	1,461

The results of the stiffness parameters from the BPE-method are shown in Table 3. The axial stiffness AE (k_{33}), the flapwise bending stiffness EI_x (k_{44}), edgewise bending stiffness EI_y (k_{55}), bend-twist coupling between flapwise bending and torsion K_f (k_{64} or k_{46}), bend-twist coupling between edgewise bending and torsion K_e (k_{65} or k_{65}), shear stiffness GAk_x (k_{11}), shear stiffness GAk_y (k_{22}) are for each element determined at the location of the elastic center and orientated according to the principle axes. The torsional stiffness GJ (k_{66}) is for each element determined at the location of the shear center.

Table 3 Main stiffness properties determined by the BPE-method.

BPE-6x6-method	Axial stiffness AE*10^6 [Nm^2]	Flapwise bending stiffness Elx*10^6 [Nm^2]	Edgewise bending stiffness Ely*10^6 [Nm^2]	Torsional stiffness GJ*10^6 [Nm^2]	Bend-twist coupling (flap + torsion) Kf*10^6 [Nm^2]	Bend-twist coupling (Edge + torsion) Ke*10^6 [Nm^2]	Shear stiffness Gakx*10^6 [N]	Shear stiffness Gaky*10^6 [N]
BPE-element 1	297,408	0,469	5,486	0,304	-0,022	0,013	38,933	8,741
BPE-element 2	343,986	0,782	7,437	0,418	-0,030	-0,014	36,879	10,187
BPE-element 3	425,033	1,372	10,669	0,698	-0,019	-0,017	40,932	12,026
BPE-element 4	515,632	2,352	14,767	0,911	-0,035	0,040	46,159	10,203
BPE-element 5	562,391	3,490	19,290	1,430	-0,073	0,149	50,583	12,102
BPE-element 6	604,993	4,960	24,482	1,970	-0,053	0,272	57,616	14,652
BPE-element 7	650,138	6,413	29,617	2,435	0,328	0,117	75,517	17,657

The bend-twist couplings are of very limited size according to the results from the BPE-method. This was expected, as the fiber layup applied for this blade would not produce bend-twist couplings of a considerable size.

The stiffnesses determined by the BPE-method are compared with stiffness properties calculated by classical Bernoulli Euler beam theory. The classical stiffnesses are determined by the relative rotations and the moment distribution over the elements.

The first and last BPE-elements are not considered because these elements are influenced by the boundary conditions.

Based on the comparison it can be concluded that there is very good agreement between the stiffness properties determined by the BPE-method and classical beam theory as shown in Figure 9.

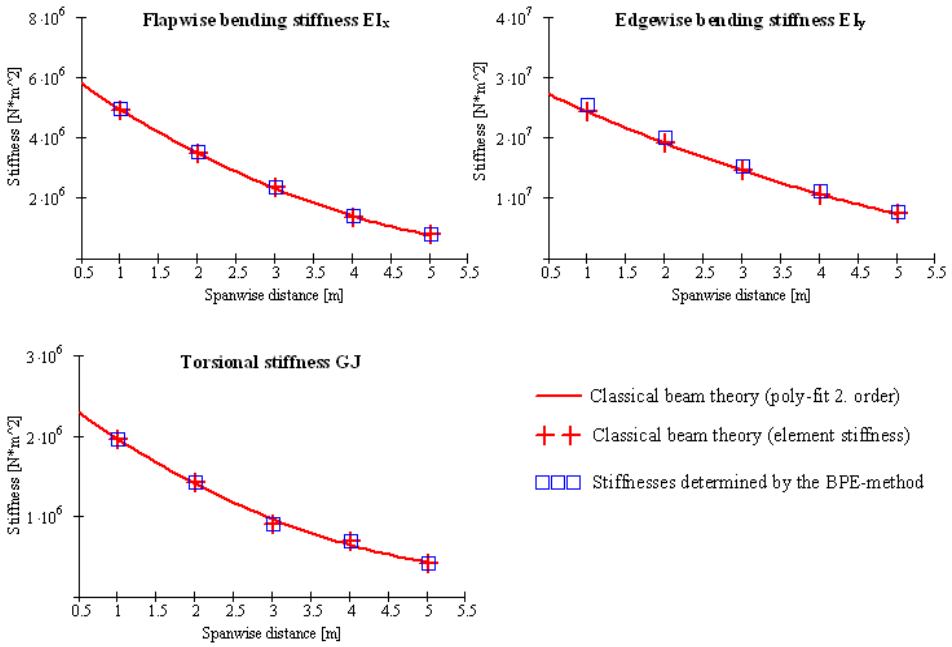

Figure 9 Compression between stiffness properties determined by the BPE-method and the stiffness determined by appling classical beam theory.

4.2.6 Results of the BPE-method applied on the bend-twist coupled blade section

In order to generate a measureble bend-twist coupling the original blade section was modified and four layers of UD1200 were laminated on the pressure and suction side. The optimal fiber angle of 25° was determined by trial and error using FEM. The additional layers were laminated as shown in Figure 10.

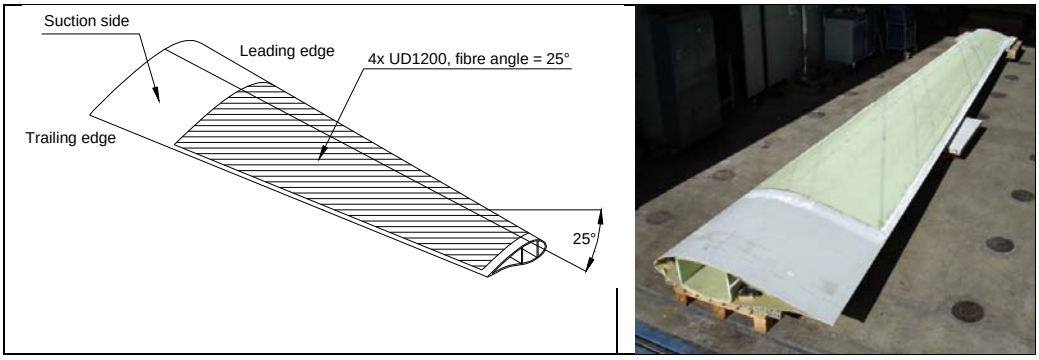

Figure 10 Left sketch of lamination of additional angled UD layers on top and bottom shells, right the picture of the physical lamination.

In order to validate the FE-model of the modified blade section a number of experimental tests were performed and compared with the numerical results. The agreement between the numerical and experimental results was excellent, for more details see Berring et al., 2007, Branner et al., 2007, Luczak et al., 2011.

The results of the stiffness parameters from the BPE-method are shown in Table 4.

The axial stiffness AE (k_{33}), the flapwise bending stiffness EI_x (k_{44}), the edgewise bending stiffness EI_y (k_{55}), the bend-twist coupling between flapwise bending and torsion K_f (k_{64} or k_{46}), the bend-twist coupling between edgewise bending and torsion K_e (k_{65} or k_{65}), the shear stiffness GAk_x (k_{11}), the shear stiffness GAk_y (k_{22}) are for each element determined at the location of the elastic center and orientated according to the principle axes. The torsional stiffness GJ (k_{66}) is for each element determined at the location of the shear center.

Since this blade section is highly coupled, the stiffness terms cannot be compared with the stiffness's known from classical beam theory.

Table 4 Stiffness properties determined by the BPE-method for the modified blade segment.

BPE-6x6-method	Axial stiffness AE*10^6 [Nm^2]	Flapwise bending stiffness Elx*10^6 [Nm^2]	Edgewise bending stiffness Ely*10^6 [Nm^2]	Torsional stiffness GJ*10^6 [Nm^2]	Bend-twist coupling (flap + torsion) Kf*10^6 [Nm^2]	Bend-twist coupling (Edge + torsion) Ke*10^6 [Nm^2]	Shear stiffness GAkx*10^6 [N]	Shear stiffness GAky*10^6 [N]
BPE-element 1	431,472	0,763	10,023	0,539	-0,145	-0,008	86,872	11,012
BPE-element 2	499,575	1,194	14,157	0,694	-0,223	-0,019	87,770	11,932
BPE-element 3	603,947	1,992	20,655	1,119	-0,306	-0,084	97,799	13,771
BPE-element 4	714,285	3,258	29,035	1,569	-0,430	0,016	109,008	12,526
BPE-element 5	781,927	4,782	38,710	2,564	-0,731	0,281	117,479	15,064
BPE-element 6	847,152	6,655	50,786	3,310	-0,928	0,780	125,824	18,449
BPE-element 7	944,462	8,286	64,951	3,951	-0,379	0,467	146,283	21,959

The additional angled UD layers should in theory create a flapwise bend-twist coupling.

The real modified blade section was experimentally tested and it was concluded that by adding these angled UD layers a measurable bend-twist coupling was generated.

The same load cases were performed experimentally and numerically on the blade section and it was concluded that the numerical response was in good agreement with the experiments.

It was therefore validated that the FE-model was able to capture the bend-twist coupled behavior.

The results of the BPE-method also show that the modified blade section has a measurable flapwise bend-twist coupling K_f.

If BPE-element 7 is not considered, it can be concluded that the bend-twist coupling decreases smoothly from the tip end to the fixed end as expected. The reason that BPE-element 7 deviates is probably due to the increasing warping resistance near the fixed end which increases the torsional stiffness and thereby minimizes the bend-twist coupling.

4.3 Full scale testing of blade section with bend-twist coupling

Earlier investigations performed by Berring et al., 2007 and Branner et al., 2007 on the blade section provided by Vestas Wind Systems A/S are continued in this study. There were generally two important issues that are presently improved: inaccurate load application in the case of torsion of the blade section and low robustness of the response measurement method using digital image correlation techniques. With the named

improvements, response of the blade section, modified as an attempt to introduce significant bend-twist coupling to the structure, to a set of applied load cases is studied.

An old-fashion hydraulic control system was utilized in the previously mentioned experimental study where the oil flow in the actuators was manually controlled by operating a valve for each actuator. Besides the problem of the actuator stroke being too short and temporarily fixation of the blade section in some load cases was needed, it was a rather good solution for such straight forward load cases like flap-wise bending or flap-wise bending and torsion where only one actuator was used and controlled at a time. However, due to the pure torsion load case was implemented as a pair of actuators placed a certain distance apart and acting at the blade section tip in two opposite directions, the problem of accurate simultaneous control of the actuators arose. Consequently, the results of the pure torsion load case were unreliable, and a principle of superposition was utilized to extract the response of the blade section in the pure torsion load case.

The results obtained by utilisation of the principal of superposition were of good quality, but still not purely experimental. This might be essential for investigations on the bend-twist coupling effects by examination of the blade section response in such load case as pure torsion, and not least because of low magnitudes of the bending deflection induced by the coupling.

In connection with inaccurate torque application experienced by Berring et al., 2007 presently a new advanced hydraulic system equipped by a couple of compact but powerful actuators is used for precise application of the required torque at the blade section tip in form of two equivalent opposite forces, see Figure 11a. Additionally, most of the load cases considered in the previous investigation are repeated and a new spar torsion load case is applied to the blade section. In the new load case the torque is applied directly to the box spar of the blade section through a specially designed handle (Figure 11b) to study possible dependence of the structural response to different torque application approaches.

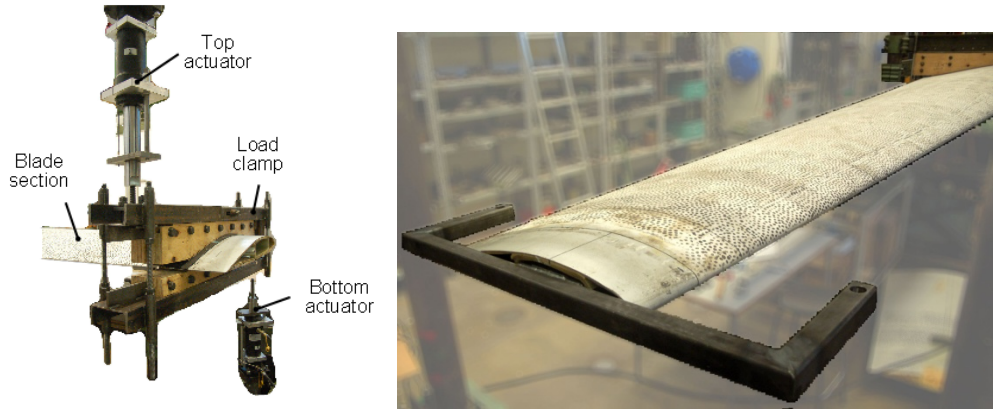

Figure 11 (a) Hydraulic actuators at the loaded clamp in the pure torsion load case. (b) Hydraulic actuators at the loaded clamp in the pure torsion load case.

The response of the blade section in the previous study was measured indirectly by processing the data obtained by a digital image correlation (DIC) system. In the present investigation it is demonstrated that the exploited data processing algorithm for calculation of bending displacements and twist angles of the blade section can potentially

introduce significant errors. A new more general and robust algorithm is developed as an improvement of the existing one.

According to the formulation of the improved DIC data processing algorithm, the bending displacement of a chosen blade cross-section is defined as the bending displacement of the point at the spar center position. Twist of the cross-section is defined as inclination of the line fitted into representation of the bending displacements of the points constituting the cross-section, see Figure 12.

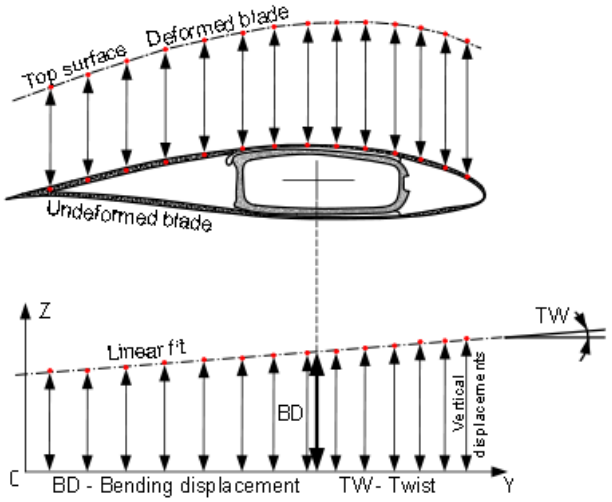

Figure 12 Visualization of the algorithm for calculation of bending displacement and twist of a cross-section.

When the pure torsion load case was accurately applied to the modified blade section, a distribution of bending displacement along the blade section length was registered. The presence of the bending displacement here is a clear proof of the effect of bend-twist coupling in the modified blade section.

The results of the spar torsion load case did not have any significant deviations from the results of the pure torsion load case. Thus, insensitivity of the blade section with respect to the pure torsion load case application approach is demonstrated.

The numerical part of the investigation on the modified wind turbine blade section consists of validation of two FE models of the blade section against the newly generated experimental results. The two models investigated are: The shell/solid FE model of the blade section developed in the previous study (Berring et al., 2007, Branner et al., 2007) and the shell FE model where the nodes of the shell elements are offset to the outer surface of the blade section. The shell/solid FE model examined here represents the best performing model according to the previous study, while the shell FE model represents one of the easiest and fastest FE models to develop.

For validation of the two FE models, bending displacements and twist angles along the blade section are calculated by application of the newly developed improved algorithm described earlier to the results of the numerical models. Thereby, the same algorithm is used for determinations of the bending displacements and twist angles along the blade section obtained experimentally and numerically.

Validation of the numerical results against the experiments exposed large deviations of the twist predicted by the shell FE model with offsets from the experimental results. This proved the problem of inaccurate prediction of the torsional stiffness by the shell FE models exploiting nodal offsets which has been highlighted in previous studies by Laird at. al., 2005 and Branner et al., 2007. The shell/solid FE model is confirmed to be the best model to predict complex response of the composite wind turbine blade structures. Further details of the experimental and numerical work are presented in Fedorov, 2012.

The general problem with material offsets in the shell element formulation has been further studied partly within this project (Dimitrov, 2008) and a solution to the problem was presented as a part of Dimitrov, 2008 based on a stiffness-matrix input approach in ANSYS. This approach is however only useful for analyzing the overall stiffness response of a turbine blade as a localized stress analysis is not possible using this approach. However, newer versions of commercial FE software such as ANSYS version 12.0, seem in the meantime to have solved the problem with shell offset, and the new shell element offset definitions in ANSYS 12.0 have been verified by the community.

4.4 Full scale testing of beams with coupling

Further experimental and numerical investigations are performed on simpler composite structures in form of uniform beams of open and closed cross-sections with introduced bend-twist coupling effect of different levels. The beams are designed as glass-fiber reinforced plastics Box- and I- shaped constant cross-section beams with flanges made of unidirectional (UD) material, see Figure 13. The beam specimens are provided by Vestas Wind Systems A/S.

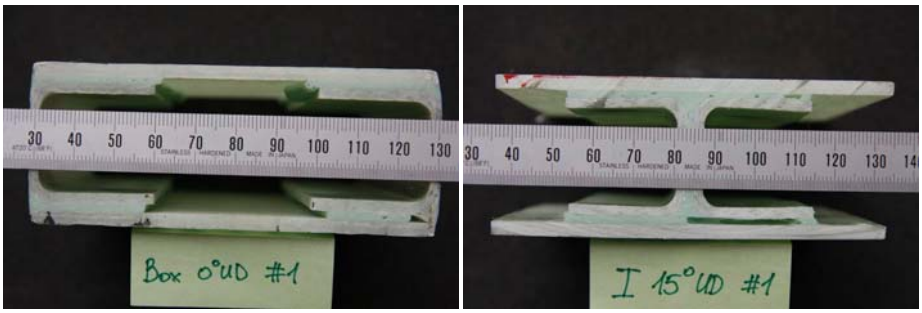

Figure 13 Box-beam and I-beam specimens.

Introduction of the bend-twist coupling into the specimens is done by variation of the fiber directions in the UD flanges. In total six unique composite beam configurations are provided for the experiments: three Box-beam configurations with 0°, 15° and 25° fiber directions in the UD flanges, and three I-beam configurations with the same fiber directions in the UD flanges.

A four-column testing machine was chosen as a platform for the experiments on the composite beams. The testing machine had possibility of mounting the specimens in the vertical position and was equipped with three hydraulic actuators for load application: a main vertical actuator and two compact actuators with possibility to be flexibly mounted in different directions. For protection of the vertical actuator from undesired off-axial loading, a new advanced test rig was designed and manufactured. The entire test setup can be seen on Figure 14.

Figure 14 Test setup for experiments on composite beams.

The composite beams are exposed to two load cases: pure torsion and pure bending. Both load cases are applied as pairs of equivalent opposite forces through the clamps mounted on the beams. The bending response in the pure torsion load case and the twist response in the pure bending load case induced by the bend-twist elastic coupling were of the particular interest in the present study.

For measurements of the beam response during the experiments three systems were exploited: a "full-scale" DIC system for measurements on the entire beam length, a "small-scale" DIC system aimed at the local part of the beam for high accuracy measurements of warping in the walls of the beams and a simple optical system for validation of the large-scale DIC measurements based on laser sources and mirrors glued on the beams for direct measurements of bending and twist angles.

For calculations of the beam bending displacements and twist angles the improved algorithm developed earlier during the investigation on the wind turbine blade section was exploited. The results obtained by processing the measurements of the large-scale DIC system by use of the algorithm were successfully validated against the direct measurements by the optical system.

The attempt of experimental measurements of warping along the composite beam walls turned out to be a success. A sine-like shape warping along the beam flanges is detected in the pure torsion load case where the twist is due to the applied torque, while in the pure bending load case, where the twist is induced by the bend-twist coupling in the beam structure, linear warping along the beam flange is detected, see Figure 15.

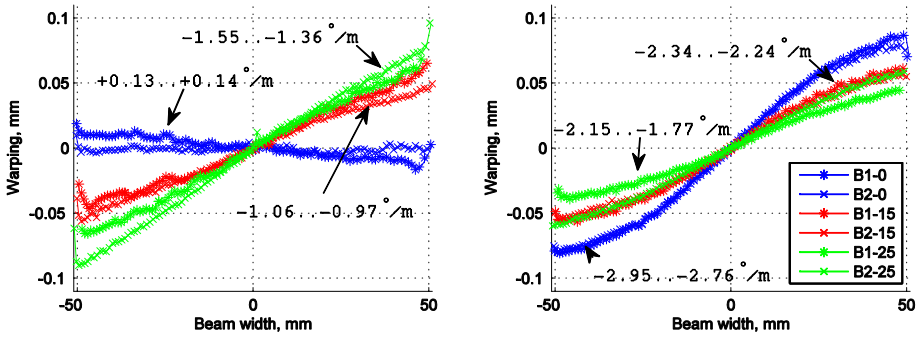

Figure 15 (a) Warping of the UD flanges of Box-beams in pure bending. (b) Warping of the UD flanges of I-beams in pure bending.

The generated experimental data is used for validation of a set of numerical models of the composite beams. There were four FE models developed for each unique beam configuration: a shell FE model with the nodal offsets to the shell outer surface, a

standard (no offsets) shell FE model, a FE model build of continuum shell elements and an FE model built of solid elements. The models are chosen as representatives of four common approaches in the development of detailed finite element models of composite structures.

The obtained numerical results are validated against the experimental data. The warping of the UD flanges was rather well predicted by the numerical models – no significant deviations from the experimental values are observed. The bending responses of all the Box- and I- beams predicted numerically are generally in very good agreement with the experiments while the twist angle distributions of the Box-beams are over predicted by all the FE models. The results of the pure torsion of the Box-beams are given in Figure 16 where it can be seen that the experimental results for all the Box-beam configurations (black lines) are in general of much lower magnitudes than the numerically predicted values (coloured). In contrast, the twist angle distributions for the I-beams are generally well predicted but the shell FE model demonstrated incorrect twist prediction as it was expected. All the other models performed rather equivalently and there are no considerable deviations among them.

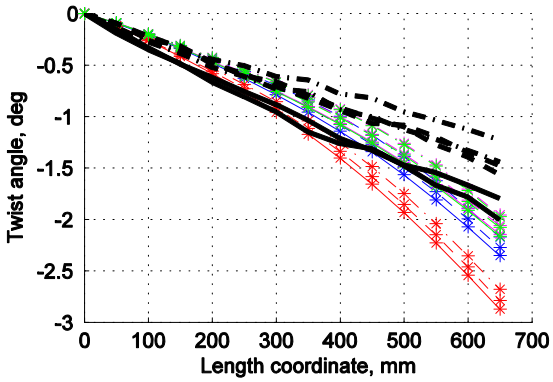

Figure 16 Twist over prediction by FE models in pure torsion of composite Box-beams.

The observed problem with incorrect prediction of the torsional response of the Box-beams is believed to be due to imperfect clamped boundary conditions applied to the beams. While the chosen solution for the beam clamping was working well in the case of the I-beams of much lower torsion rigidities, in the case of the more rigid Box-beams, the solution was not able to provide as good clamping. Further details of the experimental and numerical work are presented in Fedorov, 2012.

5 Implementation in HAWC2

This section deals with the development of the anisotropic beam element. It is shown that a typical wind turbine blade has very small couplings but that these can be introduced by adding angled unidirectional layers (see next section and Luczak et al., 2011). However, aeroelastic codes in the wind energy field, such as HAWC2, use the classical beam model. Therefore, such codes cannot be used to investigate the coupling effects of anisotropic materials.

The main aims of the present section are to develop a new beam element for the anisotropic structures and to implement the beam element into HAWC2.

5.1 Methods

Finite Element Analysis (FEA) is considered to compute a new beam element. Figure 6 shows a sketch of the coordinate system of the considered beam element.

In order to compute element stiffness and mass matrix, the elastic energy and the kinetic energy of the beam are considered. Eqs. (1) and (2) show the final form of the elastic and the kinetic energy of the beam element. More detailed expressions of the equations are addressed in Kim et al., 2012.

$$\begin{aligned} U &= \frac{1}{2}\int_0^L \varepsilon^T S \varepsilon dz' \\ &= \frac{1}{2} d^T N_\alpha{}^T \left[\int_0^L \left(B^T S B\right) dz'\right] N_\alpha d \\ &= \frac{1}{2} d^T K d \end{aligned} \tag{1}$$

$$\begin{aligned} T &= \frac{1}{2}\int_0^L \dot{r}^T E \dot{r} dz' \\ &= \frac{1}{2} \dot{d}^T N_\alpha{}^T \left[\int_0^L \left(N(z')^T E N(z')\right) dz'\right] N_\alpha \dot{d} \\ &= \frac{1}{2} \dot{d}^T M \dot{d} \end{aligned} \tag{2}$$

where U is the elastic energy, ε is the generalized strains, superscript T is transpose, S is the cross-sectional stiffness matrix, d is nodal degrees of freedom, N is the polynomial matrix, B is the strain-displacement matrix, K is the element stiffness matrix, $\dot{r}$ is the velocity of the body, E is the cross-sectional mass matrix, and M is the element mass matrix.

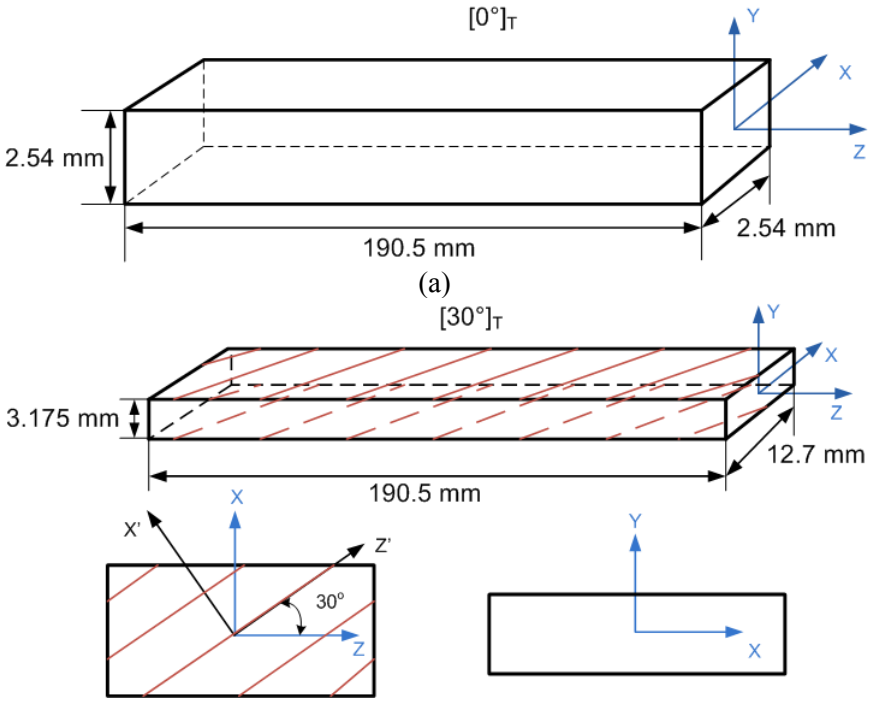

Figure 17 A sketch of considered cases. (a) Case1: $[0°]_T$ layup with arbitrary isotropic material, (b) Case2: $[30°]_T$ layup with Graphite/Epoxy.

5.2 Results

Three different cases are investigated to validate the new beam element model. The first two cases are used for validating the developed beam element with an anisotropic single body example. The last case is for dealing with a whole turbine configuration. Figure 17 shows the sketch of the Case 1 and Case 2. The last considered case is the NREL 5MW Reference Wind Turbine (RWT) (Jonkman et al., 2009).

Table 5 shows the detailed structural properties and cross-sectional stiffness matrix for the first example. For Case 2, only sectional stiffness information is displayed in Table 6. More detailed information about the material properties and geometries is addressed in Yu, 2007.

Table 5 Structural properties of Case 1 (Blasques and Lazarov, 2011).

Material	Arbitrary material
E_{11}, E_{22}, E_{33}	100 Pa
G_{12}, G_{13}, G_{23}	41.667 Pa
ν_{12}, ν_{13}, ν_{23}	0.2
ρ	1 kg/m^3
Width	0.1 m
Height	0.1 m
Length	7.5 m
Sectional stiffness of Case 1	
S_{11}, S_{22}	3.4899×10^{-1} (N)
S_{33}	1 (N)
S_{44}, S_{55}	8.3384×10^{-4} (N-m^2)
S_{66}	5.9084×10^{-4} (N-m^2)

Table 6 Sectional stiffness of Case 2.

Stiffness of Case 2 (Yu, 2007)	
S_{11}	4.4702400×10^{5} (N)
S_{13}	5.6667520×10^{5} (N)
S_{22}	3.8404032×10^{4} (N)
S_{33}	1.5861568×10^{6} (N)
S_{44}	0.1313736×10^{1} (N-m^2)
S_{46}	-9.225995×10^{-1} (N-m^2)
S_{55}	1.1656606×10^{1}(N-m^2)
S_{66}	0.1454637×10^{1} (N-m^2)

Eigenvalue analysis is performed for the three different cases. Table 7 shows the natural frequency comparisons of Case 1 between the new beam element before being implemented in HAWC2 and after implementation, respectively. They are completely identical because they are using same number of elements. From this result it may be concluded that the new beam element is successfully implemented into HAWC2.

Table 7 Natural frequency comparison of Case 1.

Mode	New beam element only [Hz]	HAWC2 [Hz]
1	2.87262E-03	2.87262E-03
2	2.87262E-03	2.87262E-03
3	1.80466E-02	1.80466E-02
4	1.80466E-02	1.80466E-02
5	5.09409E-02	5.09409E-02
6	5.09409E-02	5.09409E-02
7	1.14752E-01	1.14752E-01

Table 8 shows the natural frequency comparisons between the other existing results and a HAWC2 computation. The HAWC2 result shows good agreement with Wu, 2007. However, small discrepancies might occur due to converting the units from English to SI units and using different shape functions.

Table 8 Natural frequency comparisons of Case 2.

Mode	Case 2 HAWC2 [Hz]	Yu, 2007 [Hz]
1 (flap-torsion)	52.5	52.6
2 (edge)	209.7	209.8
3 (flap-torsion)	326.1	326.3
4 (flap-torsion)	899.3	899.8
5 (edge)	1284.2	1284.9
6 (flap-torsion)	1660.9	1661.3

It is clear to see that flapwise bending-torsion, S_{46}, and axial-edgewise deflections, S_{13}, are coupled on the structure of Case 2 from Table 6. The coupling effect on the structure can be captured through the mode shape analyses. Figure 18 shows the first 6 mode shapes of Case 2. From the mode 1, 3, 4, and 6 it is shown that the flap related modes u_y and θ_x are coupled with the torsion related mode θ_z.

From the above results of natural frequencies and mode shapes the new beam model can capture the physical behaviour of structural coupled characteristics.

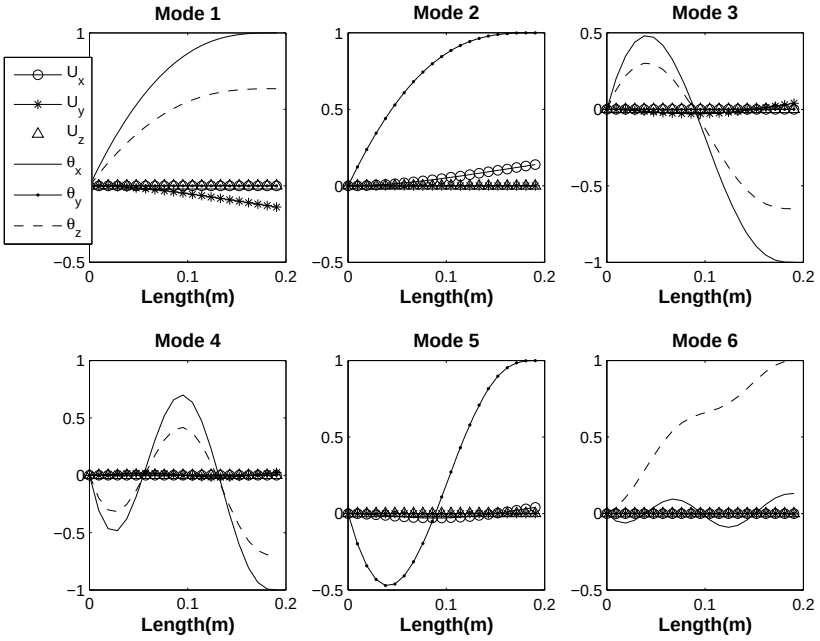

Figure 18 First 6 mode shapes of Case 2 with anisotropic properties.

In order to consider 5MW RWT the 6 by 6 cross sectional stiffness matrix are produced with the same values used for the old version of HAWC2. Eq. (3) shows how the new cross sectional values for the new beam element are obtained with the existing sectional data.

$$S_{11} = k_x GA,\ S_{22} = k_y GA,\ S_{33} = EA,\ S_{44} = EI_x,\ S_{55} = EI_y,\ S_{66} = GJ \quad (3)$$

where k_x and k_y represent shear factor for x and y direction, G and E represent shear and elastic modulus, A represents cross sectional area, I_x, I_y, and J represent area moment of inertia with respect to x- and y- axis, and torsional stiffness constant, respectively.

Table 9 shows the natural frequency comparison of 5MW RWT using the old version (i.e. before implementing the new beam model) and the new version (i.e. after implementing the new beam model) of HAWC2. All frequencies obtained show good agreement.

Table 9 Natural frequencies comparisons.

Whole turbine natural frequency [*Hz*] (structure)			Blade natural frequency [*Hz*] (body)		
	Standard version	New version		Standard version	New version
1	3.17017×10^{-1}	3.17004×10^{-1}	1	6.72048×10^{-1}	6.71166×10^{-1}
2	3.19657×10^{-1}	3.19631×10^{-1}	2	1.07864×10^{0}	1.07804×10^{0}
3	6.06803×10^{-1}	6.06571×10^{-1}	3	1.93946×10^{0}	1.93328×10^{0}
4	6.31398×10^{-1}	6.30632×10^{-1}	4	3.95532×10^{0}	3.95023×10^{0}
5	6.61957×10^{-1}	6.61118×10^{-1}	5	4.47147×10^{0}	4.46693×10^{0}
6	6.99601×10^{-1}	6.98869×10^{-1}	6	5.83890×10^{0}	5.76753×10^{0}
7	1.07370×10^{0}	1.07308×10^{0}	7	7.91385×10^{0}	7.89320×10^{0}
8	1.08798×10^{0}	1.08722×10^{0}	8	9.21933×10^{0}	9.20979×10^{0}
9	1.68962×10^{0}	1.68661×10^{0}	9	1.01272×10^{1}	1.02861×10^{1}
10	1.83475×10^{0}	1.83001×10^{0}	10	1.23857×10^{1}	1.24129×10^{1}

In this project, a new beam element which is able to consider the anisotropic behaviors is developed and implemented into HAWC2. Validations for a single body and a multibody configuration are performed with an anisotropic beam model and the 5MW RWT. Eigenvalue analyses are performed. Natural frequencies are compared between HAWC2 computations and the other existing results. The obtained results from HAWC2 are very similar to the existing ones. Mode shapes are also investigated. From the obtained results it is seen that the developed beam element is able to capture the given couplings well.

5.3 Example of load reduction

In this section a blade bending-torsion coupling effect is examined in order to investigate a load reduction potential by considering the structural couplings. For this study, the NREL 5MW RWT is considered.

Structural couplings are arbitrarily assigned based on Eq. (4) (Lobitz et al., 1998). This equation shows that diagonal stiffness terms have kept its own values while coupling effects (off-diagonal terms) are assigned. In this study only blade flapwise bending-torsion coupling is considered.

$$S = \begin{bmatrix} k_x GA & 0 & 0 & 0 & 0 & 0 \\ 0 & k_y GA & 0 & 0 & 0 & 0 \\ 0 & 0 & EA & 0 & 0 & 0 \\ 0 & 0 & 0 & EI_x & 0 & S_{BT} \\ 0 & 0 & 0 & 0 & EI_y & 0 \\ 0 & 0 & 0 & S_{BT} & 0 & GJ \end{bmatrix} \tag{4}$$

where S_{BT} is the coupling term represented as

$$S_{BT} = \alpha\sqrt{EI_x \times GJ}, \qquad -1 < \alpha < 1 \tag{5}$$

The amount of coupling is assigned by α. When α has a negative value flapwise bending toward tower results in blade twist toward feather. It is the opposite when α has a positive value. In this study two fabricated coupling cases are considered which are $\alpha = -0.05$ and $\alpha = -0.17$. Both cases are producing the bend-twist coupling for which $1m$ flapwise bending deflection resulting in approximately $0.3deg$ and $1deg$ twist at the blade tip, respectively.

A single wind speed, $7m/s$, is considered with 22% turbulence intensity. All results obtained are compared with a case with no couplings referred to as the baseline. Figure 19 shows the comparisons of the blade root flapwise, edgewise, and torsional equivalent fatigue loads and blade tip deflection. The negative sign means that the obtained values are lower than for the baseline. The S-N slope, $m = 12$, for a composite material is selected for the equivalent fatigue load analysis. Rainflow counting methodology (Matsuiski and Endo, 1968) is adapted for fatigue analysis. The blade root flapwise, edgewise, and torsional equivalent fatigue load are decreased up to approximately 2%, 0.5%, and 10%, respectively when $\alpha = -0.05$. When $\alpha = -0.17$, 20%, 0.8% and 21% of

the flapwise, edgewise, and torsional equivalent fatigue loads are reduced. The blade tip clearances are also improved for both cases, approximately 8% and 21%, respectively.

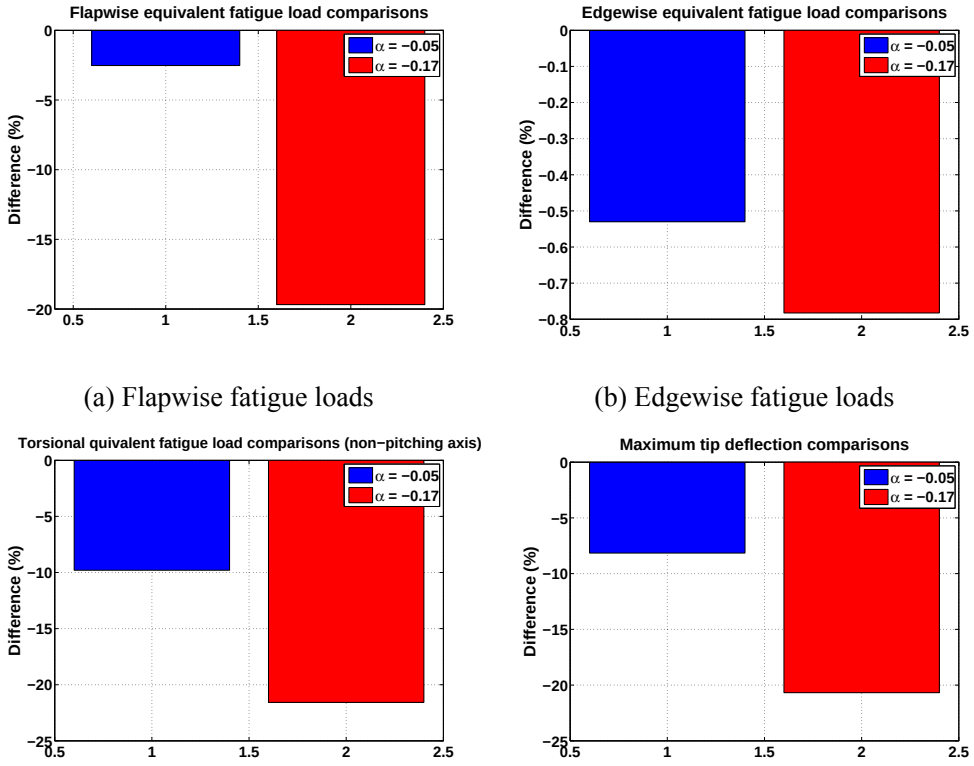

(a) Flapwise fatigue loads

(b) Edgewise fatigue loads

(c) Torsional fatigue loads

(d) Maximum blade tip deflections

Figure 19 Equivalent fatigue loads and maximum blade tip deflection when $\alpha = -0.05$ *and* $\alpha = -0.17$.

From this parametric study it is evident that a structural coupling can improve turbine performances by for instance reducing loads and improving blade tip clearance as well.

6 Blade couplings in practice

6.1 Couplings obtained for I- and box-beams

In the present study a simplified method for analysis on bend-twist coupling in the beam structures is developed. The foundation for the method was found in a work by Chandra et al., 1990. There, for bend-twist coupled beams, a simple formulation was used in form of 2x2 matrix to describe the relation between the applied load (M – bending moment, T - torque) and the beam response (w'' - bending curvature, φ' - twist rate). The matrix incorporated only bending stiffness EI, torsional stiffness $GJ$and the bend-twist coupling coefficient K. Further, the normalized coupling coefficient α was derived by Lobitz and Veers, 1998:

$$\begin{Bmatrix} M \\ T \end{Bmatrix} = \begin{bmatrix} EI & -K \\ -K & GJ \end{bmatrix} \begin{Bmatrix} w'' \\ \varphi' \end{Bmatrix} \qquad \alpha = \frac{-K}{\sqrt{EIGJ}}$$

This formulation was used by Lobitz and Veers, 1998, Lobitz and Veers, 2003 and Ong and Tsai, 1999 in their research on elastic coupling in composite structures. In the developed simplified bend-twist coupling analysis method, the 2x2 constituting matrix formulation by Chandra et al., 1990 is accommodated for application to the experimental results obtained by exploiting DIC techniques and numerical results of highly detailed FE models built of shell- and/or solid elements. Thereby, by applying a bending moment and a torque to a numerical model of the beam and by measuring the beam response in form of bending curvatures and twist rates distributions, distributions of bending stiffness, torsional stiffness and normalized bend-twist coupling coefficient can be obtained based on the simplified formulation above. The same method can be used in the experiments when a DIC system is utilized.

The developed algorithm is adopted for the experimental studies where the DIC system is utilized for the measurements. The adaptation is based on a great advantage of the DIC system which is able to provide vast amounts of measured data along the beam length to overcome the problem of low robustness of the determination of bending curvatures and twist rates in form of derivatives of the measured bending displacements and twist angles along the beam.

The simplified bend-twist coupling analysis method is validated against the VABS and BECAS tools. A benchmark case of solid beam with significant coupling is considered where the bending and torsional stiffnesses together with the coupling coefficient calculated by the developed simplified analysis method are compared to the results of VABS and BECAS tools. A very good agreement is demonstrated for the bending stiffness and only moderate deviations up to 8% are found for the torsional stiffness and coupling coefficient.

Further, the developed simplified analysis method is applied to a numerical model of the blade section investigated earlier and compared to the results of the beam property extraction method developed by Laird et al., 2005 and applied to the blade section by Berring et al., 2007 and Branner et al., 2007. Generally, good agreement between the results for the bending stiffness calculated by the two methods was found. The results of torsional stiffness and bend-twist coupling coefficient did not agree well which can be explained by the principal differences between the response calculation methods exploited in the two analyses.

Additionally, the developed analysis method is applied to the numerical and experimental results for the composite beams reported in section 4.4. The results of the bending and torsional stiffnesses together with be coupling coefficient obtained numerically are validated against the experimental results. Generally good agreement is found for the bending stiffness but significant deviations are observed for the torsional stiffness – in accordance with the results obtained earlier during the study on composite beams, see Figure 20. The new analysis method provided direct evaluations of the variations of the stiffnesses and the coupling coefficient along the beam specimens, which clearly exposed the problem of imperfect clamping in the Box-beams. The method also provided the coupling coefficient variations along the beam specimens. The normalized coefficient α obtained experimentally was found to be of ca. 0.3 and 0.4 for the 15° and 25° UD Box-beams accordingly and of ca. 0.1 for both 15° and 25° UD I-beams.

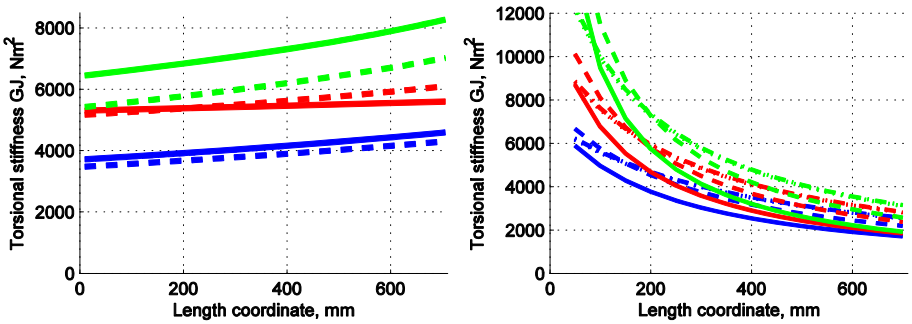

Figure 20 (a) Experimentally obtained torsional stiffness of Box-beams. (b) Numerically predicted torsional stiffness of Box-beams. Blue - 0 deg. UD, red - 15 deg. UD, green - 25deg. UD.

6.2 Couplings obtained for a traditional wind turbine blade

An extensive literature study is performed to overview the achievable magnitudes of the bend-twist elastic coupling in form of the normalized bend-twist coupling coefficient for the composite beams of different geometries: from simple plates to real wind turbine blades. It was found that the bend-twist coupling coefficient magnitude is heavily affected by the material properties. When highly anisotropic carbon fibre reinforced plastics (CFRP) material is exploited, much higher values of the bend-twist coupling can be obtained in comparison to the situation where the glass fibre reinforced plastics (GFRP) material is used.

It is demonstrated that when a common approach to introduce the bend-twist coupling by directing the fibers away from the beam longitudinal axis is used, the normalized bend-twist coupling coefficient has a clear trend towards lower practically achievable values when the composite beam structures change from simple plates (values of 0.5 for GFRP and 0.8 for CFRP) to realistic wind turbine blades where the magnitude of the coupling is generally limited by 0.2 for the GFRP and 0.4 for the CFRP.

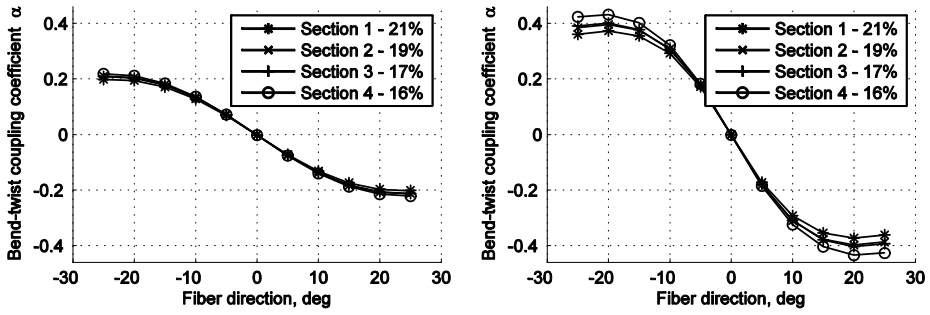

Figure 21 Variation of the normalized bend-twist coupling coefficient of wind turbine blade sections. (a) GFRP. (b) CFRP.

To evaluate the practical limits of the bend-twist elastic coupling in a real wind turbine blade structure a numerical investigation is carried out on the Vestas wind turbine blade section studied earlier. Several cross-sections corresponding to the airfoils of different thicknesses (16%-21%) are selected for the study and FE models of long uniform beams

of the selected cross-sections are developed. The bend-twist coupling was introduced to the structures by variation of the UD GFRP material in the spar flanges in the range of 0°..25°. Additionally, a substitution of the UD GFRP material with the CFRP material with the fibres varied in the same range is studied. Using the developed simplified bend-twist coupling analysis method, variations of the bending and torsional stiffnesses and the normalized bend-twist coupling coefficient due to the fibre direction variation are obtained, see Figure 21. It is demonstrated that the maximal value for the normalized bend-twist coupling coefficient is of 0.2 for the GFRP material with 25° fibre direction and of 0.4 for the CFRP material with 20° fibre direction. The achieved results correspond well to the results of the literature survey which is considered to be a good indication of the obtained values to be the practical limits of the bend-twist coupling in the wind turbine blade structures.

6.3 Automatic generation of input for the cross-section analysis software BECAS

Real world wind turbine blades feature a complex geometry and a complex material layup. Therefore, it is important that the input for cross-section analysis tools like BECAS is produced automatically and in a consistent and reproducible way.

For this purpose the python program shellexpander was further developed within in the ANBAVI project. Shellexpander generates input files for BECAS based on information contained in a finite element shell model. Finite element shell models of wind turbine blades are routinely set up using a variety of software tools and are often readily available.

The input required by BECAS for each cross-section comprises a 2D-mesh of the cross-section and the corresponding material and orientation assignments. It is assumed that the finite element shell model uses layered shell elements, and that the nodes of the shell model are offset to the outer surface of the blade.

Each shell element is converted into a stack of three-dimensional solid elements by “expansion” in the local normal direction. The two-dimensional mesh for BECAS is then found by projecting the back faces of the three-dimensional elements to an appropriate plane. 4-node and 8-node quadrilateral shell elements result in 4-node and 8-node quadrilateral BECAS elements respectively.

Figure 22 shows part of a finite element shell model of a wind turbine blade. Figure 23 shows one of the 2D meshes generated by shellexpander based on the shell model.

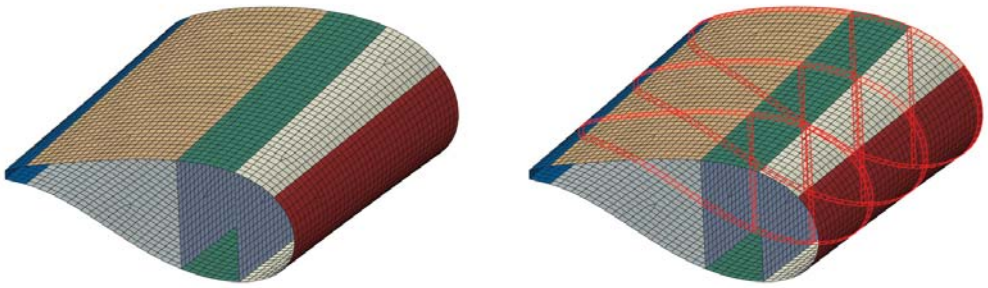

Figure 22 (a) Part of a finite element shell model of a wind turbine blade. (b) Three element sets defining three cross-sections that are analyzed by BECAS.

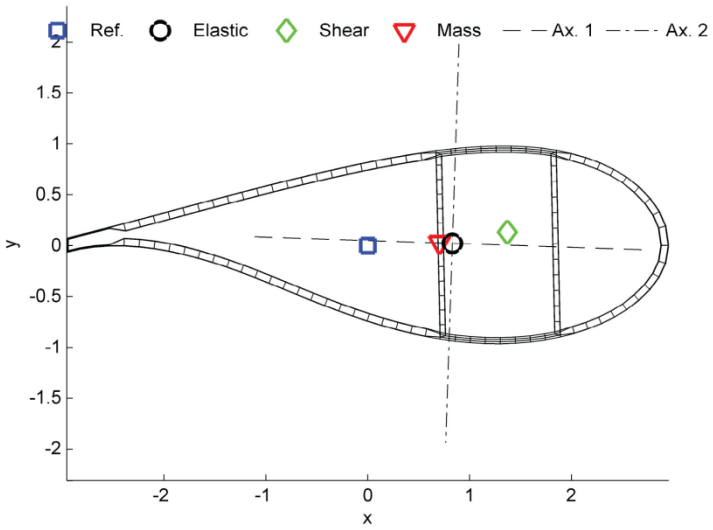

Figure 23 2D mesh generated by shellexpander. The center of mass, shear center, elastic center and the elastic axes are also indicated.

As layup and thickness information in the finite element shell model is usually defined on an element basis, thickness discontinuities occur. In order to facilitate mesh generation, shellexpander removes these discontinuities by defining a continuous, node-based thickness distribution. This is achieved by defining the thickness at a node as the minimum, maximum or average thickness of any shell element attached to this node.

In addition to the algorithm described above the node-based thickness distribution can be controlled by defining dominant element sets. If dominant element sets are specified, the node-based thickness distribution at thickness discontinuities is governed by the dominant elements.

6.4 Example: Analyzing a bend-twist coupled blade using BECAS and Shellexpander

In this section the ability of BECAS to predict the cross-section properties of bend-twist coupled wind turbine blades is demonstrated by means of an example.

An existing finite element shell model of an 89m long rotor blade was used. Bend-twist coupling was introduced by rotating the fibres in both caps by 20 degree for r>44m. The blade is loaded in flap-wise direction by a distribution of concentrated forces. The response of the blade is analyzed using a finite element beam model based on the cross-sectional properties computed by BECAS. Figure 24 shows the deformation predicted by the beam model together with the respective cross-sections.

Current work is focusing on the comparison of the results obtained from the beam model to corresponding finite element shell models.

It must be highlighted that the finite element shell model has approximately 2000000 degrees of freedom, while the beam model has only 960.

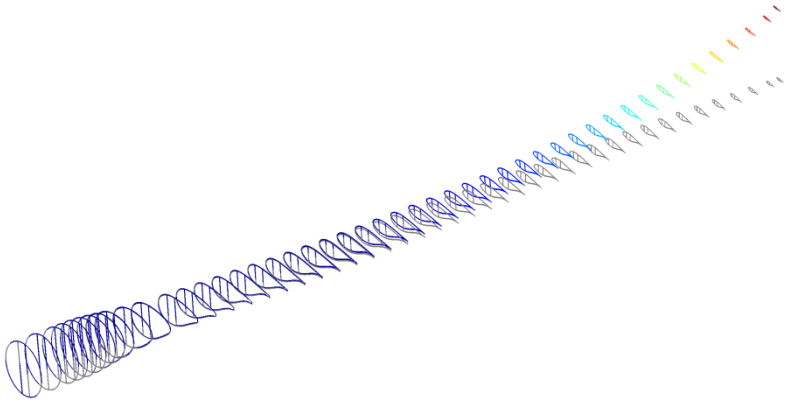

Figure 24 Deformation of the bend-twist coupled blade as predicted by the finite element beam model.

7 Discussion and conclusions

In this project (ANBAVI), supported by the Danish Energy Authority through the 2007 Energy Research Programme (EFP 2007), a general, fully coupled beam element has been developed, validated and implemented in the aeroelastic code HAWC2.

A cross section analysis tool BECAS (BEam Cross section Analysis Software) has also been developed and validated in the project. BECAS is able to correctly predict all geometrical and material induced couplings and the tool has obtained great interest from both industry and academia.

Another method to calculate structural couplings from detailed finite element models and experiential measurements has also been studied and further developed in this project. The method is called the BPE(Beam Property Extraction)-method.

The results from the project now make it possible to use structural couplings in an intelligent manner for the design of future wind turbine blades. It has already been shown in a small parameter in this project that there is a possibility to reduce fatigue loads using structural couplings. However, more work is needed before these possibilities are fully explored and blades with structural couplings can be put in production.

The developed beam element is especially developed for wind turbine blades and can be used for modeling blades with initial curvature (pre-bending), initial twist and taper. Originally, we had an idea to include non-linear deformation of the cross section but this has shown to be too ambitious and will require must more research before it is possible.

The developed fully coupled beam element and cross section analysis tool has been validated against both numerical calculations and experiential measurements. Numerical validation has been performed against beam type calculations including Variational Asymptotical Beam Section Analysis (VABS) and detailed shell and solid finite element analyses. Experiential validation includes specially designed beams with built-in couplings, a full-scale blade section originally without couplings which later was modified with extra composite layers in order to obtain measurable couplings. Both static testing and dynamic modal analysis tests have been performed.

Cross sectional layout and material properties have been studied to see the effect on the Brazier effect and buckling. This work did not arrive at a stage where it can be published. Finally, it have been studied what size of structural couplings that can be obtained in current and future blade designs.

The theory underlying the evaluation of the cross section stiffness properties is briefly described in this report. The numerical implementation of the theory has been subsequently addressed. Finally, the validation of BECAS was presented. The cross section stiffness properties estimated by BECAS have been compared against VABS (the Variational Asymptotic Beam Section Analysis by Yu et al., 2002a). Results are presented for different combinations of solid, thin-walled and open cross sections, and isotropic and layered orthotropic materials. It is shown that the results from BECAS match exactly those of VABS in all cases. In particular, BECAS is able to correctly predict all geometrical and material induced couplings which is a typical challenge for this type of tool. These results strongly suggest that BECAS is an efficient and robust cross section analysis tool able to handle a large range of section geometries and material properties.

The results from the BPE-method were subjected to some uncertainties as the cross sections became asymmetric and anisotropic. The constitutive matrices from the BPE-method should in theory be symmetric, but as these cross sections became asymmetric and anisotropic these matrices were not completely symmetric. This indicates that the BPE-method is not computing the completely correct constitutive matrix. It is not clear what causes this asymmetric in the constitutive matrices but it seems that it is primarily related to the shear deformation because the asymmetric terms are primarily located in the first two columns and rows in the constitutive matrices. The reason could also be that it is too simple to assume that a cross section with hundreds of degrees-of-freedom can be described by single set of rotations and displacements (three rotations and displacements).

8 Publications

8.1 Publications from current project

Berring P., Branner K., Berggreen C. and Knudsen H.W., 2007, Torsional performance of wind turbine blades – part I: Experimental investigation, in: Proc. of 16th International Conference of Composite Materials, 8-13 July 2007, Kyoto, Japan.

Blasques J.P., 2012, Multi-material topology optimization of laminated composite beams with eigenfrequency constraints, (submitted).

Blasques, J.P., Lazarov, B., 2011, A Cross Section Analysis Tool for Anisotropic and Inhomogeneous Sections of Arbitrary Geometry. Risø-R-1785.

Blasques J.P., Stolpe M., 2009, Maximum stiffness optimization of composite beams for wind turbine applications, Proceedings of the 8th World Congress on Structural and Multidisciplinary Optimization, Lisbon, Portugal.

Blasques J.P., Stolpe M., 2010, Maximum stiffness and minimum weight optimization of laminated composite beams using continuous fiber angles, Structural and Multidisciplinary Optimization, DOI: 10.1007/s00158-010-0592-9.

Blasques J.P., Stolpe M., 2012, Multi-material topology optimization of laminated composite beam cross sections, (submitted).

Branner K., Berring P., Berggreen C. and Knudsen H.W., 2007, Torsional performance of wind turbine blades – part II: Numerical verification, in: Proc. of 16th International Conference of Composite Materials, 8-13 July 2007, Kyoto, Japan.

Dimitrov, N., 2008, Methods for Analysing Torsion Stiffness of Wind Turbine Blades - Initial Study, Master Thesis, Department of Mechanical Engineering, Technical University of Denmark, Kgs. Lyngby, Denmark.

Fedorov, V.A., 2012, Structural Modeling of Wind Turbine Blades with Passive Control, PhD Thesis, Department of Wind Energy, Technical University of Denmark, Kgs. Lyngby, Denmark.

Fedorov, V.A., Dimitrov, N., Berggreen, C., Krenk, S., Branner, K. & Berring, P., 2009, Investigation of Structural Behavior Due to Bend-Twist Couplings in Wind Turbine Blades, in: Proc. of 17th International Conference of Composite Materials (ICCM), 27-30 July 2009, Edinburgh, UK.

Fedorov, V.A., Dimitrov, N., Berggreen, C., Krenk, S., Branner, K. & Berring, P., 2010, Structural Behaviour Due to Bend-Twist Couplings in Wind Turbine Blades, NAFEMS Nordic Seminar, 2 - 3 February 2010, Esbjerg, Denmark.

Kim, T. & Branner, K., 2011, Anisotropic Beam Element for Modeling of the Wind Turbine Blades, in: Proc. of European Wind Energy Conference and Exhibition (EWEA), 14-17 March 2011, Brussels, Belgium.

Kim, T., Branner, K. & Hansen, A.M., 2011, Developing Anisotropic Beam Element for Wind Turbine Blade Design, in: Proc. of 18th International Conference of Composite Materials (ICCM), 21-26 August 2011, Jeju Island, Korea.

Kim, T., Branner, K. & Hansen, A.M., 2011, Parametric Study of Composite Wind Turbine Blades, in: Proc. of 32nd Risø International Symposium on Materials Science, 5-9 September 2011, Roskilde, Denmark.

Kim, T., Hansen, A.M. & Branner, K., 2012, Development of an Anisotropic Beam Finite Element for Composite Wind Turbine Blades in Multibody System, Wind Energy (submitted)

Luczak, M., Branner, K., Berring, P., Manzato, S., Haselbach, P. & Peeters, B., 2011, Experimental Verification of the Implementation of Twist-bend Coupling in a Wind Turbine Blade, in: Proc. of European Wind Energy Conference and Exhibition (EWEA), 14-17 March 2011, Brussels, Belgium.

Luczak, M., Branner, K., Kahsin, M., Martyniuk, K., Peeters, B. & Ostachowicz, W., 2010, Applying static and dynamic test responses for defect prediction in wind turbine blades using a probabilistic approach, in: Proc. of European Wind Energy Conference and Exhibition (EWEC), 20-23 April 2010, Warsaw, Poland.

Luczak, M., Manzato, S., Peeters, B., Branner, K., Berring, P. & Kahsin, M., 2011, Dynamic Investigation of Twist-bend Coupling in a Wind Turbine Blade, Journal of Theoretical and Applied Mechanics, Volume 49 Issue 3, pp. 765-789.

Luczak, M., Peeters, B., Mevel, L., Döhler, M., Ostachowicz, W., Malinowski, P., Wandowski, T. & Branner, K., 2010, Damage Detection in Wind Turbine Blade Panels

Using Three Different SHM Techniques, in: Proc. of IMAC XXVIII, 1-4 February 2010 Florida, USA.

Luczak M., Peeters B., Szkudlarek W., Mevel L., Döhler M., Ostachowicz W., 2009, Branner K., Martyniuk K., Comparison of the three different approaches for damage detection in the part of the composite wind turbine blade, in: Proc. of IWSHM 2009, 9-11 September 2009, Stanford, CA, USA.

Szkudlarek W., Kahsin M., Luczak M., Peeters B., Kurowski M., Branner K., Martyniuk K., Wasilczuk M., 2009, Vibration-Based Damage Detection In Multilayer Composite Material, in: Proc. of ICSV16, 5-9 July 2009, Krakow, Poland.

Sørensen, B. F., Holmes, J. W., Brøndsted, P. & Branner., K., 2010, Blade Materials, Testing Methods and Structural Design, Chapter 13 in Wind Power Generation and Wind Turbine Design (edited by Dr. Wei Tong), WIT Press.

8.2 Other publications

Borri M., Ghiringhelli G. L., Merlini T., 1992, Linear analysis of naturally curved and twisted anisotropic beams, Composites Engineering, (2)5-7, 433-456.

Borri M., Merlini T., 1986, A large displacement formulation for anisotropic beam analysis, Meccanica, (21), 30-37.

Chandra, R., Stemple, A. D. and Chopra, I., 1990, Thin-walled composite beams under bending, torsional, and extensional loads, Aircraft, 27(7):619-626.

Chaviaropoulos, P.K., et al., 2006, Enhancing the damping of wind turbine rotor blades - the DAMPBLADE project, Wind Energy, 9, 163-177.

Chen H., Yu W., Capellaro M., 2010, A critical assessment of computer tools for calculating composite wind turbine blade properties, Wind Energy, (13)6, 497-516.

Ganguli R., Chopra I., 1995, Aeroelastic optimization of a helicopter rotor with composite coupling, Journal of Aircraft, 32(6), 1326-1334.

Ghiringhelli G. L., 1997a, On the thermal problem for composite beams using a finite element semi-discretization, Composites Part B, (28B), 483-495.

Ghiringhelli G. L., 1997b, On the linear three dimensional behaviour of composite beams, Composites Part B, (28B), 613-626.

Ghiringhelli G. L., Mantegazza P., 1994, Linear, straight and untwisted anisotropic beam section properties from solid finite elements, (4)12, 1225-1239.

Ghiringhelli G. L., Masarati P., Mantegazza P., 1997, Characterisation of Anisotropic, Non-Homogeneous Beam Sections with Embedded Piezo-Electric Materials, Journal of Intelligent Material Systems and Structures, (8)10, 842-858.

Giavotto V., Borri M., Mantegazza P., Ghiringhelli G., Carmaschi V., Maffiolu G.C., Mussi F., 1983, Anisotropic beam theory and applications, Composite Structures, (16)1-4, 403-413.

Hansen M. O. L., Sørensen J. N., Voutsinas S., Sørensen N., Madsen H. A., 2006, State of the art in wind turbine aerodynamics and aeroelasticity, Progress in Aerospace Sciences, (42), 285-330.

Jonkman J, Butterfield S, Musial W, Scott G., 2009, Definition of a 5-MW Reference Wind Turbine for Offshore System Development. Technical Report NREL/TP-500-38060, February 2009.

Jung S. N., Nagaraj V. T., Chopra I., 1999, Assessment of composite rotor blade modeling techniques, Journal of the American Helicopter Society, (44)3, 188-205.

Laird, D., Montoya, F. and Malcolm, D., 2005, Finite element modeling of wind turbine blades, in Proceedings of the AIAA/ASME Wind Energy Symposium, 10-13 January 2005, Reno, Nevada, pp. 9-17.

Li L., Volovoi V. V., Hodges D. H., 2008, Cross-sectional design of composite rotor blades, Journal of the American Helicopter Society, 53(3), 240-251.

Lobitz, D. and Veers, P., 1998, Aeroelastic behavior of twist-coupled HAWT blades, in Proceedings of the AIAA/ASME Wind Energy Symposium, 12-15 January 1998, Reno, Nevada.

Lobitz, D. and Veers, P., 2003, Load mitigation with bending/twist-coupled blades on rotors using modern control strategies, Wind Energy, 6(2):105-117.

Malcolm, D.J. and Laird D.L., 2005, Identification and Use of Blade Physical Properties, in Proceedings of the ASME/AIAA Wind Energy Symposium, 10-13 January 2005, Reno, Nevada.

Matsuiski M. and Endo T., 1968, Fatigue of metals subjected to varying stress. Japan Society of Mechanical Engineering, Fukuoka, Japan.

Ong, C. and Tsai, S., 1999, Design, Manufacture and Testing of a Bend-Twist D-Spar, Technical Report SAND99-1324, Sandia National Laboratories, Albuquerque, NM.

Yu, W., 2007, Efficient High-Fidelity Simulation of Multi-body Systems with Composite Dimensionally Reducible Components. Journal of the American Helicopter Society; 52(1): pp. 49-57.

Yu W., Hodges D.H., Volovoi V., Cesnik C. E. S., 2002a, On Timoshenko-like modelling of initially curved and twisted composite beams, International Journal of Solids and Structures, (39), 5101-5121.

Yu W., Volovoi, V.V., Hodges D.H., Hong X., 2002b, Validation of the Variational Asymptotic Beam Sectional Analysis (VABS), AIAA Journal, (40)10, 2105-2113.

Volovoi V.V., Hodges D.H., Cesnik C.E.S., Popescu B., 2001, Assessment of beam modeling methods for rotor blade applications, Mathematical and Computer Modeling, (33), 1099-1112.

DTU Wind Energy
Technical University of Denmark

Frederiksborgvej 399
4000 Roskilde
Denmark
Phone +45 4677 5024

www.vindenergi.dtu.dk